Article:

Pradhan, B, Sarhosis, V orcid.org/0000-0002-8604-8659, Ferrotto, MF et al. (2 more authors) (2021) Prediction Equations for Out-of-Plane Capacity of Unreinforced Masonry Infill Walls Based on a Macroelement Model Parametric Analysis. Journal of Engineering Mechanics, 147 (11). 04021096. ISSN 0733-9399

https://doi.org/10.1061/(ASCE)EM.1943-7889.0001998

Prediction Equations for the Out-Of-Plane Capacity of Unreinforced Masonry Infill Walls Based on a Macro-element Model Parametric Analysis

Bharat Pradhan[1], Vasilis Sarhosis[2], Marco F. Ferrotto*[1], Davorin Penava[3], Liborio Cavaleri[1]

[1]*Department of Engineering, University of Palermo, Viale delle Scienze, 90128 Palermo, Italy*

[2]*School of Civil Engineering, University of Leeds, LS2 9JT, Leeds, United Kingdom*

[3]*Faculty of Civil Engineering and Architecture, University of Osijek, 3 Vladimir Prelog Str., 31000 Osijek, Croatia*

*corresponding author email: marcofilippo.ferrotto@unipa.it

Abstract

In the seismic performance assessment of reinforced concrete (RC) frames, a reliable estimation of the capacity of unreinforced masonry (URM) infill walls is of utmost importance to ensure structural safety conditions. With particular attention to the Out-of-Plane (OoP) capacity of URM infill walls after In-Plane (IP) damage, the issue of defining reliable analytical prediction models for the assessment of the capacity is an ongoing study. In this paper, empirical equations are proposed for the evaluation of the infilled frame's OoP capacity, with or without IP damage, based on an extensive numerical parametric analysis, focusing on the influence of the key parameters that govern the mechanical model. The OoP capacity of URM infill walls, considering the variation in their geometrical and mechanical properties, was evaluated by using a macro-element model. The OoP strength was found to be largely influenced by compressive strength, slenderness ratio, aspect ratio, and additionally by the level of IP damage. The reduction of OoP strength and stiffness due to IP damage was largely governed by the strength and the slenderness ratio of the URM infill wall. The reliability of the proposed model was also proved by comparisons with experimental results and some of the analytical models already available in the literature. The proposed equations provide reliable estimates of the OoP capacity, by strongly indicating the suitability of the adopted macro-element model in capturing the OoP response of URM infills.

Keywords: Macro-element model, RC frame, URM infill wall, OoP capacity, IP/OoP interaction, seismic performance, parametric study

1. Introduction

Unreinforced masonry (URM) infill walls in reinforced concrete (RC) frame structures are highly vulnerable to earthquakes. During seismic events, masonry infills are prone to damages in both in-plane (IP) and out-of-plane (OoP) directions (Braga et al. 2011; Ricci et al. 2011; Varum et al. 2017). The costs of reparing are usually very high and the downtime is significant (Del Vecchio et al. 2018; De Risi et al. 2019a). Further, the OoP collapse of masonry infills represents a large threat to life safety. This has led to an increase of the studies related to the OoP behaviour of infill walls in recent years.

The critical influence of the masonry infills on strength, stiffness and ductility of frame structures subjected to seismic actions is an important issue highlighted for several years by the researchers and widely addressed (Papia et al., 2003, Di Trapani et al., 2015, 2018). Recently, strategies of improvement of infilled structures' seismic capacity have been studied too, based on the introduction of dissipative devices (Zahrai et al. 2015; Castaldo et al. 2021).

Differently from the IP coupling between frame and infill and the modification of frame behaviour because of infills, the problem of IP/OoP behaviour interaction of infills, especially the change in the OoP strength of infills that experienced previous IP damage, has got high attention in both experimental investigations (Ricci et al. 2018a, 2018b; De Risi et al. 2019b; Butenweg et al. 2019, Di Domenico et al. 2021) and numerical studies (Cavaleri et al. 2019; Donà et al. 2019; Ricci et al. 2019, Wang et al. 2020) only in the last ten years.

The first studies related immediately the OoP strength of infill walls to the development of an arching action. This effect relies on the compressive strength of masonry and the slenderness ratio (*ratio of height to thickness*) of infill walls (e.g. McDowell 1956a, 1956b). Subsequently, many researchers proposed analytical equations to estimate the OoP capacity based on the arching action (Dawe and Seah 1989; Angel 1994; Bashandy et al. 1995; Flanagan and Bennett 1999b; Moghadam and Goudarzi 2010). However, many of the capacity models available in the literature provide a high scatter in the estimation of infills' OoP capacity (Anić et al. 2019), raising the question of their reliability. Although the compressive strength of masonry and the slenderness ratio of infill walls have been proven to be the response key parameters, there is great uncertainty about them. For example, infill walls made with hollow masonry units usually have differences in their mechanical properties (e.g. compressive strength) in horizontal and vertical directions. Likewise, the slenderness ratio changes with the thickness of the infill wall and also according to the masonry infills' aspect ratio (*ratio of length to height*). The increase in the aspect ratio increases the slenderness in the horizontal direction and consequently decreases the OoP capacity (Moreno-Herera et al. 2016; De Risi et al. 2019b). Equally important is the stiffness of the frame surrounding the masonry infills in the development of the arching mechanism (Angel 1994).

Several experimental studies have shown that masonry infills can have adequate resistance to OoP seismic loads (e.g. Dawe and Seah 1989; Angel 1994; Flanagan and Bennett 1999a). More importantly, several researchers have highlighted that damage in the IP direction reduces OoP capacity of masonry infills (Angel 1994; Calvi and Bolognini 2001; Da Porto et al. 2013; Hak et al. 2014; Ricci et al. 2018a, 2018b; De Risi et al. 2019b). This has been evident from the performance of masonry infills in recent earthquakes as well (e.g. 2019 Durrës, Albania).

Fig 1. OoP collapse (left) and IP damage of URM infill walls on RC frame multi-storey building during 2019 Durrës, Albania earthquake (courtesy of ACI Technical Committee 133 - Disaster Reconnaissance building survey task force)

The OoP collapse of masonry infills is often observed at lower to intermediate storeys rather than at the top, where higher OoP acceleration is expected. This is due to IP/OoP interaction effects: higher IP damage occurs in the masonry infills in the lower floors and, as a consequence, they are easily ejected out by OoP seismic (inertial) forces. The damage due to IP loading includes the modification of the frame-infill connection. It is well known that due to IP lateral loads, infills partially detach from the frames (Polyakov 1960; Holmes 1961; Stafford Smith and Carter 1969; Mainstone 1971, 1974; Liau and Kwan 1984; Paulay and Priestley 1992; Saneinejad and Hobbs 1995). This fact modifies the OoP performance of infills during earthquakes (e.g. Paulay and Priestley 1992; Decanini et al. 2004; De Luca et al. 2013, Longo et al. 2016). Therefore, IP load changes the frame-infill boundary conditions, whose modification may increase the risk of early OoP collapse (Butenweg et al. 2019). Unfortunately, in spite of boundary conditions between frame and infill affect the failure modes (Anić et al. 2019), few experiments have investigated such effects (e.g. Dawe and Seah 1989; Di Domenico et al. 2018, 2019; Butenweg et al. 2019).

Another aspect to point out is that, according to the nature of the seismic input, IP and OoP loads act simultaneously in general. Loss of OoP strength due to simultaneous IP and OoP loads can be higher with respect to consider IP loading independent from OoP loading as is done generally during the experimental tests. An experimental study by Flanagan and Bennett (1999a) under the combined action of IP and OOP loads (as a simpler form of simultaneous loads) resulted in reduced OoP capacity compared to the sequential application of IP and OoP loads. However, the quantification of the difference between sequential and simultaneous IP and OoP loads is still difficult due to the lack of experiments.

Different proposals for the decay of OoP strength due to IP damage are available in the literature. Since most of them are proposed based on very few tests, there is no convergence of the results when compared with each other (Cavaleri et al. 2019). Also, the differences are influenced by the nature of the experiments as every experimentation has its inherent characteristics (e.g. test setups and loadings/boundary conditions, etc). Angel (1994) and Ricci et al. (2018b) emphasized the role of slenderness ratio in the OoP strength decay, while many others expressed the strength decay relation by keeping it simple depending only on the level of IP damage (Morandi et al. 2013; Verlato et al. 2014; Akhoundi et al. 2018; Furtado et al. 2018b; Ricci et al. 2018a; Cavaleri et al. 2019). Lately, Di Domenico et al. (2021) proposed a strength decay equation by additionally including the aspect ratio. From the above discussion, it is clear that several parameters have to be considered to describe the OoP capacity of infill walls. However, the influence of each parameter is not easy to be defined. The main difficulty is also the lack of experimental tests in a wide range of variations in geometrical and mechanical properties of masonry infills. In this context, a systematic study of the influence of the key parameters is possible only through numerical investigations. Partially, FE-based micro-models have been used to deepen the understanding of the OoP behaviour of URM infill walls and the aspect of the IP-OoP interaction (Agnihotri et al. 2013; Cavaleri et al. 2019; Liberatore et al. 2020; Wang et al. 2020).

Agnihotri et al. (2013) investigated the influence of slenderness ratio and aspect ratio on OoP capacity and also their influence on strength reduction due to the IP damage. They concluded that the variation in the rate of strength decay is higher due to a change in the aspect ratio rather than the change in the slenderness ratio. According to them, infill walls with a higher aspect ratio show a higher decay rate with increasing IP damage. Additionally, they showed a high reduction of OoP strength even at small IP drift (e.g. more than 50% for an IP drift of 0.15% for a wall with a slenderness ratio of 16) which is not convincing when compared to experimental results.

Wang et al. (2020) concluded that the reduction of OoP strength due to IP damage is influenced by slenderness ratio, aspect ratio, and additionally by the masonry strength which was not previously considered by others. The strength reduction was lower for masonry infills with higher compressive strength but the stiffness decay was found not affected by the masonry strength. According to them, infills with a higher slenderness ratio are affected by a higher reduction of strength/stiffness at the same level of IP damage. Additionally, the rate of strength decay was lower for masonry infills with a higher aspect ratio in contrast to the idea of Agnihotri et al. (2013). This shows that the reduction of OoP strength/stiffness of infills is still not sufficiently understood and needs further investigation. In this paper, a macro-element model (Pradhan and Cavaleri 2020) has been used to perform a parametric analysis to investigate the OoP strength of infill walls bounded closely by frames on all sides. The reason being, the chosen model is able to handle the variation of masonry infill properties easily and at the same time, it is much faster in computation compared to micro-models which makes it appropriate when detailed parametric investigation like this has to be carried out. Different lengths, heights, and thickness of infill walls have been considered along with variations in the mechanical properties of masonry. OoP capacity has been determined with or without considering the IP damage. To consider the IP damage, OoP load has been applied after the application of IP load, but not simultaneously (the model has been proved to be reliable with respect to the available tests characterized by a sequential application of IP and OoP loads). Based on the numerical results, empirical equations have been proposed to estimate the OoP strength of the infill wall considering the influence of masonry strength, slenderness ratio, aspect ratio, and IP damage. Additionally, a decay law has been proposed for OoP stiffness. The accuracy of the proposed equations has been checked with the experimental results.

2. Description of the macro-element model

The numerical modelling was carried out by using the macro-element model of Pradhan and Cavaleri (2020). The model was validated with several experimental results (Angel 1994; Calvi and Bolognini 2001; Da Porto et al. 2013; Ricci et al. 2018a, 2018b; De Risi et al. 2019b) covering a range of masonry infills' geometrical and mechanical characteristics. In this macro model, the infill wall is represented by four struts (two diagonals, one horizontal and one vertical). Each strut is modelled by two fiber section beam-column elements connected by a node at the mid-span as shown in Fig 2.

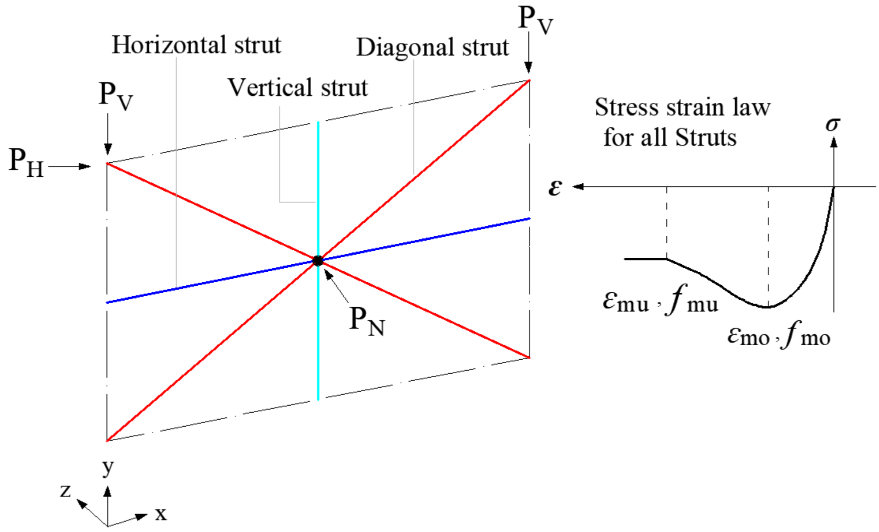

Fig 2. Macro-element model (Pradhan and Cavaleri 2020)

In the model, the width of the diagonal struts w_d, horizontal strut w_h and vertical strut w_v are calculated by the following equations:

$$w_d = d/3 \quad [1a]$$

$$d = \sqrt{l'^2 + h'^2} \quad [1b]$$

$$w_h = h - w_d / \cos\theta \quad [1c]$$

$$w_v = l - w_d / \sin\theta \quad [1d]$$

where l and h are the clear length and height of the infill wall respectively, while l' is the centre to centre distance between the columns and h' indicates the height from the center of lower beam to the centre of top beam. The Greek letter θ is the angle defining the slope of the diagonal struts. In order to accurately represent both IP and OOP resistances of an infill wall, the width and the thickness of diagonal, vertical and horizontal struts, before defined by Eq. 1, are replaced by surrogated values. The surrogated equivalent struts maintain the same cross-sectional area as the original struts. For any of the struts with width w and thickness t, the surrogated width $\overline{w}$ and the surrogate thickness $\overline{t}$ are derived in the following ways:

$$\bar{w} = \frac{f_{mo}}{f_m} \times w \qquad [2a]$$

$$\bar{t} = \frac{f_m}{f_{mo}} \times t \qquad [2b]$$

The mechanical property of the strut fibers in compression is defined by using four stress strain parameters, namely, f_{mo}, f_{mu}, ε_{mo} and ε_{mu} as shown in Fig 2. Among the parameters, f_{mo} and ε_{mo} can be calculated based on the value of equivalent compressive strength f_m and elastic modulus E_m of the masonry according to the following equations provided in Pradhan and Cavaleri (2020).

$$f_{mo} = 0.61 + 0.0001 f_m E_m - 10^{-9} (f_m E_m)^2 \qquad f_m E_m < 40000 \qquad [3a]$$

$$\varepsilon_{mo} = 4 \times 10^{-8} f_m E_m + 0.00039 \qquad [3b]$$

In the above equations, $f_m E_m$ is the product of the two properties f_m and E_m. The ultimate stress f_{mu} is taken as 60% of peak stress f_{mo} and the ultimate strain corresponding to ultimate stress ε_{mu} can be defined with a value of $10 \times \varepsilon_{mo}$.

The equivalent properties of masonry, f_m and E_m have to be derived by considering the mean directional properties following the equations 4a and 4b.

$$f_m = \sqrt{f_{mh} \times f_{mv}} \qquad [4a]$$

$$E_m = \sqrt{E_{mh} \times E_{mv}} \qquad [4b]$$

where f_{mv} and f_{mh} represent the compressive strength of masonry in the vertical and horizontal directions, and E_{mv} and E_{mh} are the elastic modulus of masonry in the vertical and horizontal directions respectively. This provision facilitates the model to consider the orthotropic nature of masonry.

In the macro-element model, OoP resistance of any strut is proportional to the compressive strength of masonry and the strut width, further it reduces when the slenderness ratio of the strut increases. This makes the OoP resistance of the diagonal, vertical, and horizontal struts different. More specifically, diagonal struts have the biggest role while the horizontal strut has the least contribution in OoP resistance. The scenario can be different for an IP-damaged infill wall because the OoP resistance of diagonal struts decreases gradually with increasing level of IP damage (please refer to Pradhan and Cavaleri 2020 for more details on the macro-element model).

In the case of low thickness infill walls, the OoP strength is small and, although the role of horizontal and vertical struts in the OoP strength is comparatively lower than that of the diagonal struts, they are necessary to derive the full OoP strength as proved by a comparison with experimental tests (contribution of each strut in the OoP capacity can be checked in Pradhan and Cavaleri 2020). On the other hand, as the thickness of the infill wall becomes big, OoP strength provided by horizontal and vertical struts also increases. Particularly, OoP resistance due to vertical strut also becomes significant in such cases and, numerically obtained OoP strength may be overestimated. It was confirmed after the comparison with some available experimental results on thick infill wall specimens (e.g. Flanagan and Bennett 1999a, Hak et al. 2014) .

The easiest way to address such conditions is to eliminate the vertical strut from the model, as this strut (like the horizontal one) contributes only in OoP resistance and not in IP resistance of infilled frames. Figs 3 & 4 show the numerical response obtained by using the macro-element model for such cases, with and without the vertical strut (related experimental data are in Table 1 and the geometrical and mechanical parameters for the struts identified following the procedure described above are provided in Table 2).

As any numerical model, the one here used is affected by uncertainties related to the geometrical and mechanical properties of infills and surrounding frames (Celarec and Dolšek 2013; Holický et al. 2016; Castaldo et al. 2019; Di Domenico et al., 2019 Castaldo et al. 2020). However, the difference between prediction and experimental result has been proved to be always limited (Pradhan and Cavaleri 2020).

The macro-element model here used is applicable for infill walls surrounded by sufficiently stiff frames and is not appropriate for the case of any gap between frame and infill, which prevents full activation of arching action (the terms of applicability of the model have been discussed in Pradhan and Cavaleri 2020).

For the current study, to avoid a possible overestimation of the OoP capacity and in agreement o the experimental results available in the literature, the vertical strut has been dropped from the macro-element model, when the thickness of the infill is equal to or greater than 200 mm.

Table 1. Geometrical and mechanical properties of the infill wall obtained from the experiments

Experiments	l mm	h mm	t mm	f_{mh} MPa	f_{mv} MPa	E_{mh} MPa	E_{mv} MPa
Flanagan and Bennett (1999a)	2240	2240	200	3	5.6	2300	5300
Hak et al. (2014)	4222	2950	350	1.08	4.64	499	5299

Table 2. Geometrical and mechanical properties of struts used for numerical simulations

Experiments	$\overline{w}_d$ mm	$\overline{w}_v$ mm	$\overline{w}_h$ mm	$\overline{t}$ mm	f_{mo}	f_{mu}	ε_{mo}	ε_{mu}
Flanagan and Bennett (1999a)	490	310	310	446	1.84	1.10	0.00096	0.0096
Hak et al. (2014)	791	428	299	816	0.96	0.58	0.00054	0.0054

The numerical modelling was performed in OpenSees (McKenna et al. 2000). Frame elements, as well as strut elements, were modelled by using fiber-section beam-column elements with distributed plasticity. The behaviour of concrete and infill masonry was modelled using Concrete02 material, while the steel reinforcement was simulated by using Steel02 material available in OpenSees platform. Concrete02 is an uniaxial stress-strain concrete material with tensile strength and linear tensile softening. In the current study, zero tensile strength has been assumed according to Mander et al. (1988). The concrete confinement due to transverse reinforcement is not taken into account. Similarly, Steel02 is a uniaxial steel material with isotropic strain hardening based on Menegotto-Pinto model (Menegotto and Pinto 1973). A distinct layer has been defined in the fibers of the frame elements to model longitudinal reinforcements. Concrete02 material is combined with MinMax material available in OpenSees to simulate the failure of fibers in the struts by dropping the corresponding stress to zero when the ultimate strain is achieved. According to the thickness of the infills, struts' arrangement was automatically configured in the numerical model by interfacing Matlab and OpenSees in which the former is used to pass the geometrical and mechanical parameters of the struts as well as the IP drift level to OpenSees. To consider the effect of IP damage in the OoP capacity, IP load was applied to achieve predefined inter-storey drift levels before the application of OoP load. Simultaneous application of IP and OoP loads is not considered because the model is calibrated on experiments characterized by a non contemporary application of IP and OoP load. The IP displacement was imposed at the top of the masonry infilled frame while the OoP load was applied at the middle of the struts.

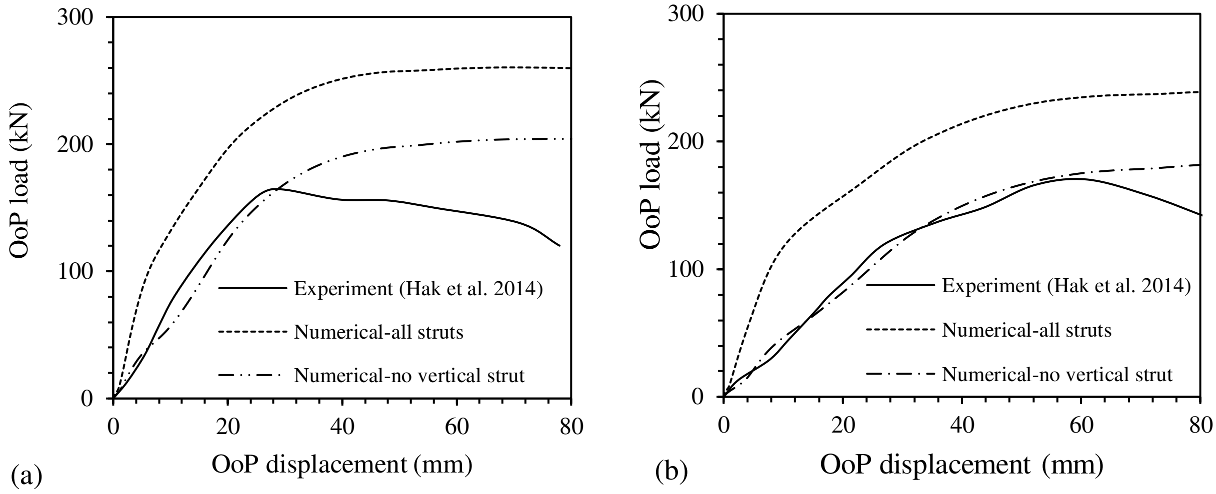

Fig 3. Experiments in Hak et al. (2014) - infill thickness 350 mm - OoP response obtained with and without the vertical strut: (a) OoP load after 1% of IP drift; (b) OoP load after 1.5% of IP drift.

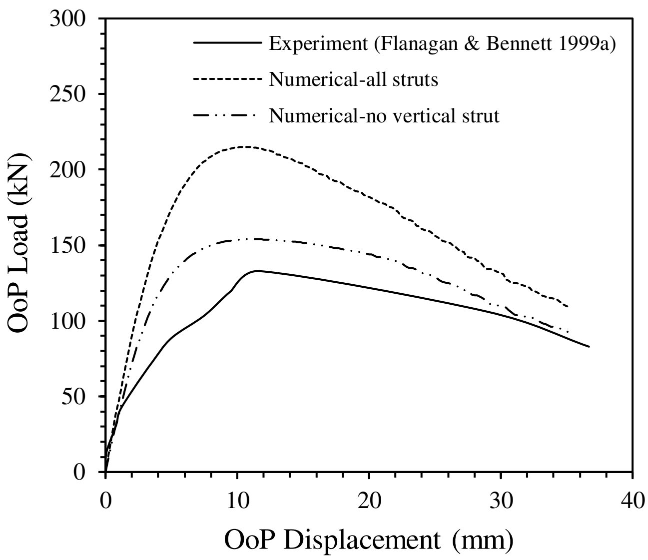

Fig 4. Experiment in Flanagan and Bennett (1999a) - infill thickness 200 mm - OoP response with and without the vertical strut - load only in OoP direction.

3. Parametric analysis and discussion of results

3.1 Ranges for the parameters investigated

The parametric analyses have been performed by varying geometrical and mechanical properties of masonry infills. Three different heights of infill walls were considered i.e. 2400 mm, 2600 mm, and 2800 mm. For each infill wall height, five different aspect ratios were assumed (1.0, 1.25, 1.5, 1.75, and 2). To vary the aspect ratio, length of the infill wall was changed by keeping the height constant for each infill wall height considered. The thicknesses of masonry infills were varied from 80 mm to 300 mm (with an increment of 20 mm) thus making a higher variation in the slenderness ratios (i.e. 8 to 35). The mechanical characteristics of the masonry, namely compressive strength and elastic modulus, were also varied. The equivalent compressive strength (defined as above by Eq. 4-a) was taken in the range from 1 to 6 MPa (step of 0.5 MPa) and the elastic modulus was assumed as 1000 times the compressive strength of masonry, as shown in Table 3. Additionally, the stiffness of the bounding frames was varied by changing the dimension of the columns (*size of beam and column as shown in Table 3*). The investigated frames were representative of framed structures complying with the seismic requirements of the contemporary building design codes.

The OoP strength of URM infill walls was determined by considering both the IP damaged and the IP undamaged conditions. The IP drift was taken as a measure of the IP damage and was defined by different values of inter-storey drift ratio, or simply IDR (range from 0 to 2% with an increasing step of 0.25%). To cause the IP damage, a single cycle of IP load was applied to each masonry infilled frame before the application of the OoP load. The numerical analysis was performed by using the macro-element model described in the previous section. The details of the different parameters considered in the study are summarised in Table 3.

Table 3. Parameters considered for numerical modelling

Frame measures		Concrete		IP drift	Infill wall measures			Masonry	
Column size (width×depth) mm×mm	Beam size mm×mm	f_c MPa	E_c MPa	IDR %	height h mm	Aspect ratio l/h	thickness t mm	f_m MPa	E_m MPa
300 ×300, 450×300, 600×300, 750×300 300×450, 300×600, 300×750	300×400	30	27500	0 to 2 step (0.25)	2400 2600 2800	1, 1.25, 1.5, 1.75, 2	80 – 300 step (20)	1 to 6 step (0.5)	1000×f_m
Reinforcement content in columns	2% of the cross-section area with minimum 3 rebars in the shorter side and uniformly distributed along the longer side -Transverse ties with 8 mm rebars @ 100 mm c/c						Yield strength of rebar = 500 MPa		
Reinforcement content in beams	1% of the cross-section area with 3 rebars at the top and bottom -Transverse ties with 8 mm rebars @ 100 mm c/c								

3.2 Influence of infill wall thickness and masonry strength

The OoP capacity of infill walls was highly influenced by the variation of its thickness and of masonry strength as well. The increase of thickness from 100 to 300 mm caused the increase of the OoP capacity by almost 8 times, independently by the masonry compressive strength f_m. In other words, as the slenderness ratio (h/t) becomes lower, the OoP capacity becomes higher. For the same thickness of the infill wall, the OoP capacity increases when as the masonry compressive strength increases as well. The OoP capacity was almost 5 times higher when masonry strength was increased from 1 MPa to 6 MPa for any infill thickness.

In Fig 5 a-c, the numerical outputs for some specific thicknesses of infill walls at specific values of masonry strengths are shown. These results are for the case of aspect ratio (l/h) of infills equal to 1. The curves in the figures highlight the effect of masonry strength and thickness of infill walls. These figures also indicate that with the increase in the infill area (i.e. increase in height and length of infill walls), the OoP capacity decrease. This is due to the increase of the slenderness ratio in both, the vertical and the horizontal directions. From the discussion, it is obvious that with the increase in the infill aspect ratio, OoP capacity decreases.

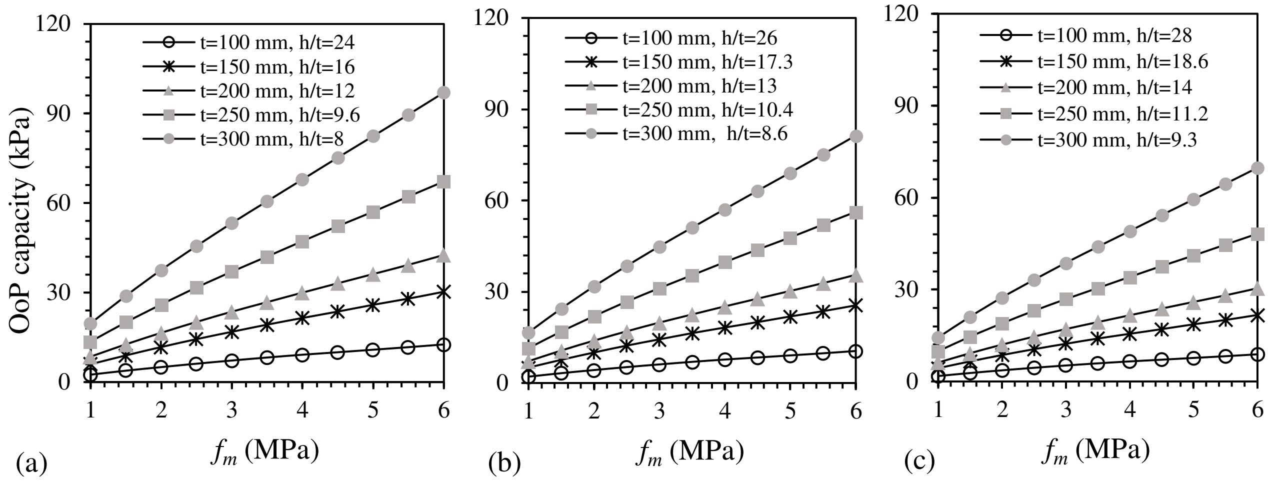

Fig 5. OoP capacity of infill walls depending upon masonry strength and infill wall thickness, slenderness ratio and size: a) *l*=*h* =2400 mm; b) *l*=*h*=2600 mm; and c) *l*=*h*=2800 mm

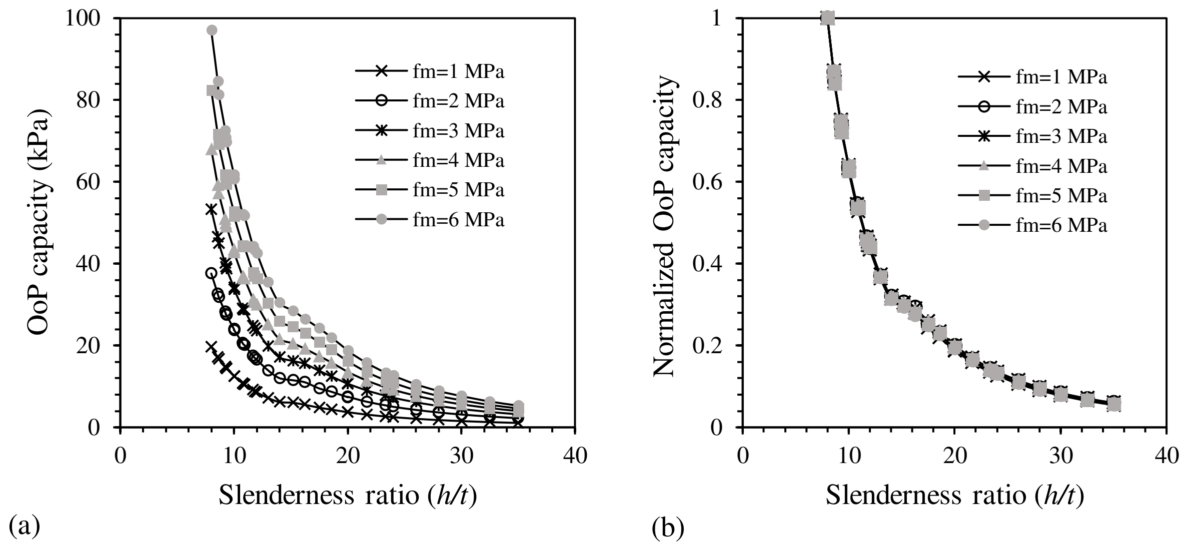

Fig 6. OoP capacity of infill walls depending upon slenderness ratio and masonry strength (a); OoP capacity normalized with respect to the maximum one corresponding to the minimum slenderness ratio (b).

In Fig 6-a, results are plotted in terms of the slenderness ratio of infills. It can be observed that the OoP strength is very low when the slenderness ratio increases beyond 20 (EC8 limit is 15). The results clearly indicate that the OoP capacity is proportional to the strength of masonry. The results are consistent with the original concept of arching provided by McDowell et al. (1956a, 1956b). In addition, Fig 6-b highlights that the reduction ratio of OoP strength due to the increasing slenderness ratio is not influenced by the strength of masonry. In Fig. 7, for a better understanding, a 3D representation of the results in Fig. 6-a can be found .

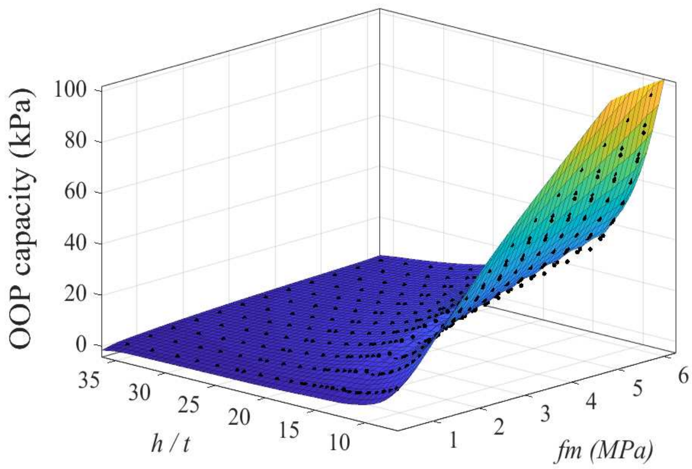

Fig 7. OoP capacity of infill walls versus masonry strength f_m and slenderness ratio h/t

3.3 Effect of aspect ratio

In Figs 8-10, the variation of OoP capacity due to the variation of the aspect ratios of infills is shown, for different thickness and strengths of masonry and for the case of infill walls having a height of 2600 mm. From Figs 8b, 9b & 10b, it is highlighted that the reduction of OoP strength of infill walls due to increasing of the aspect ratio is not influenced by the masonry strength and the thickness (or slenderness ratio) of infill walls. Upon increasing the aspect ratio from 1 to 1.5, OoP capacity decreased to about 60% and, when the aspect ratio was equal to 2, OoP capacity dropped to almost 40% on average. The trend was similar for the infills with different height (2400 mm and 2800 mm). A comparison of OOP capacities at different aspect ratios for infills of different heights, thickness, and masonry strengths is kept in Fig 11.

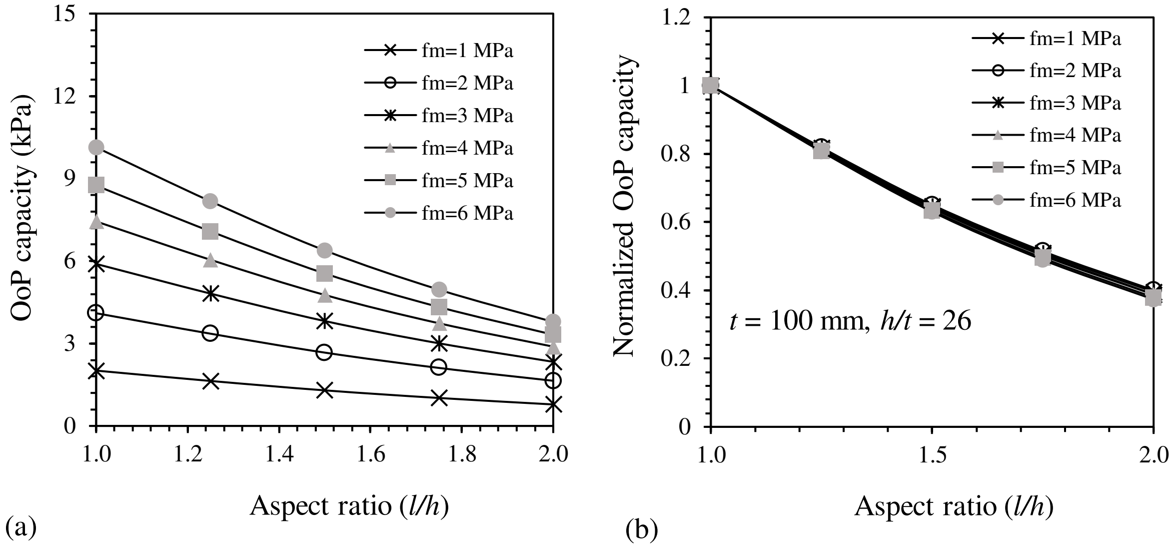

Fig 8. OoP strength vs aspect ratio for different values of masonry strength - t = 100 mm, h = 2600 mm, h/t = 26 - (a); OoP capacity normalized with respect to the maximum one corresponding to the minimum aspect ratio (b)

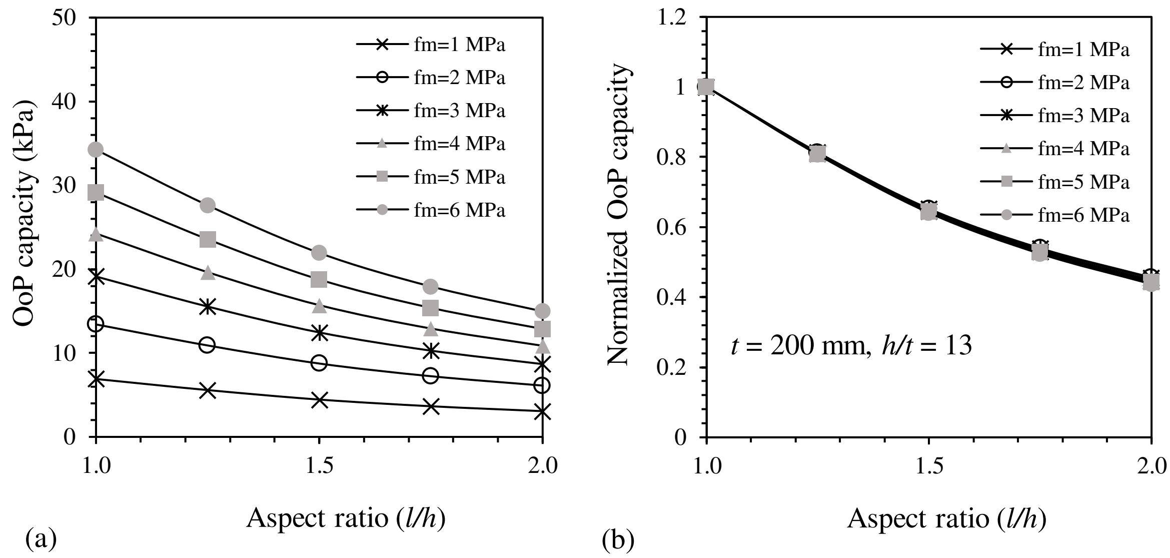

Fig 9. OoP strength vs infill aspect ratio for different values of masonry strength - t = 200 mm, h = 2600 mm, h/t = 13 (a); OoP capacity normalized with respect to the maximum one corresponding to the minimum aspect ratio (b).

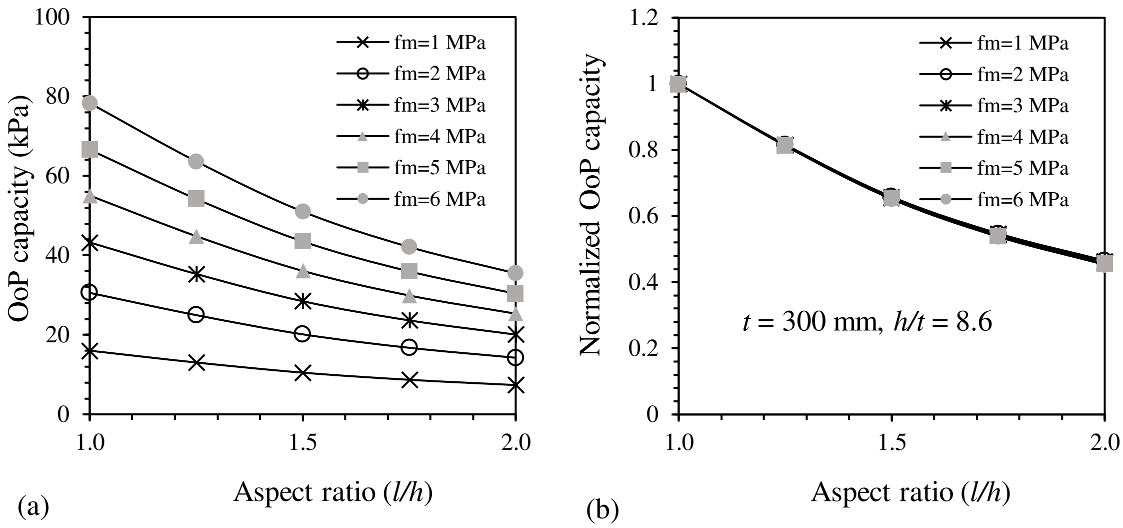

Fig 10. OoP strength vs infill aspect ratio - t = 300 mm, h = 2600 mm, h/t = 8.6 – (a); OoP capacity normalized with respect to the maximum one corresponding to the minimum aspect ratio (b).

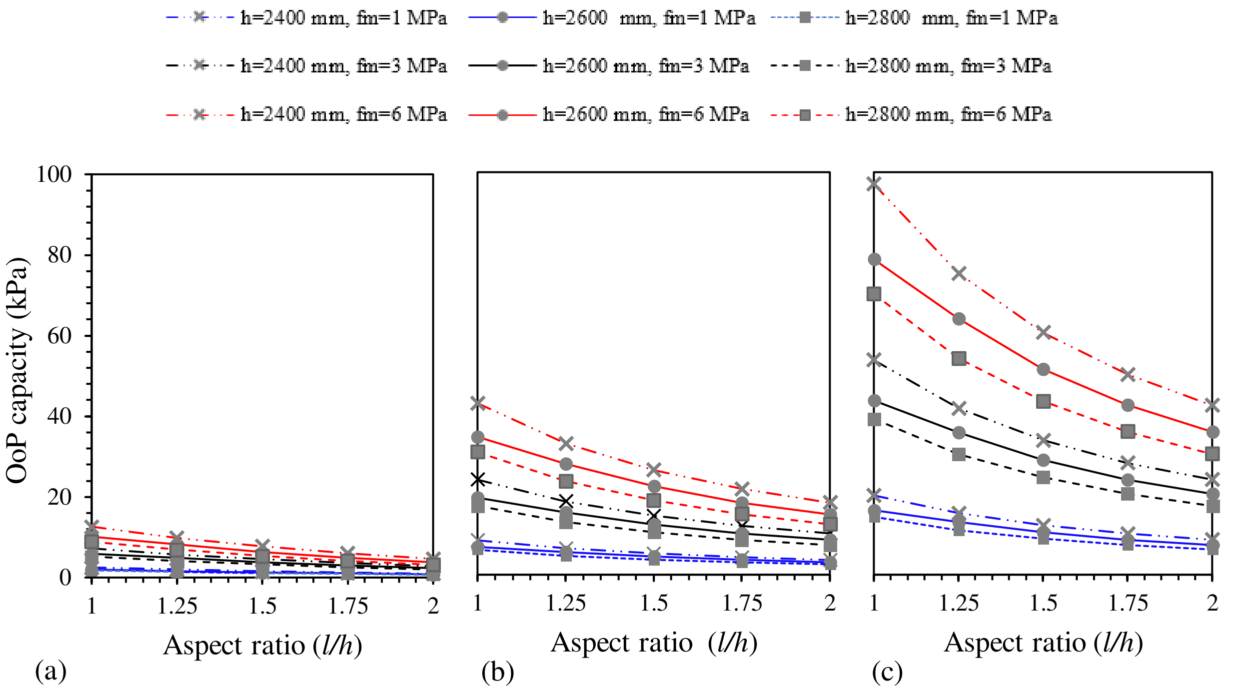

Fig 11. Comparative OoP strength vs infill aspect ratio for different infill heights and strength of masonry: a) t=100 mm; b) t=200 mm; c) t=300 mm

3.4 Decay of OoP strength and stiffness

The numerical results showed that the reduction of OoP strength due to IP damage can vary according to the strength of masonry and the thickness (or slenderness ratio) of infills. The decay of strength with increasing IP drift is lower for thicker and stronger masonry. Such conclusion was also reached by Wang et al (2020) from their numerical study. As an example, the particular case of an infill wall (height =2600 mm) having an aspect ratio of 1.0 is shown in Figs 12-15. These figures clearly show that at the same level of IP damage, strength decay is lower when the strength of masonry is higher. Particularly in Fig 15, the decay of OoP strength according to infill wall thickness (or h/t), at different strengths of masonry, is compared. Fig.15 shows that the decay of OoP strength is higher when the slenderness ratio is higher. Fig 15-a also indicates that for a low strength of masonry, the reduction of OoP capacity is less influenced by h/t values. In summary, the strength decay of infill walls characterized by lower h/t values, for an assigned level of IP damage, is lower in the case of higher strength of masonry. In Fig 16, the OoP capacities of infill walls having different heights and having aspect ratio 1 at various levels of IP drifts are kept together for comparison.

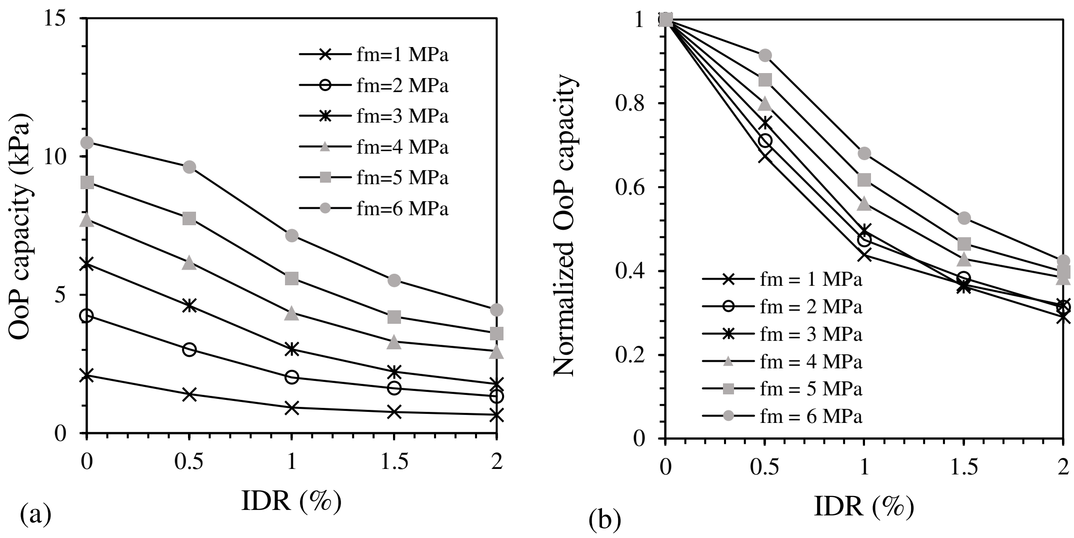

Fig 12. Decay of OoP capacity of infill walls vs IP drift - *l*=*h*=2600 mm, *t* = 100 mm (*h/t*=26) - (a); normalized OoP capacity.

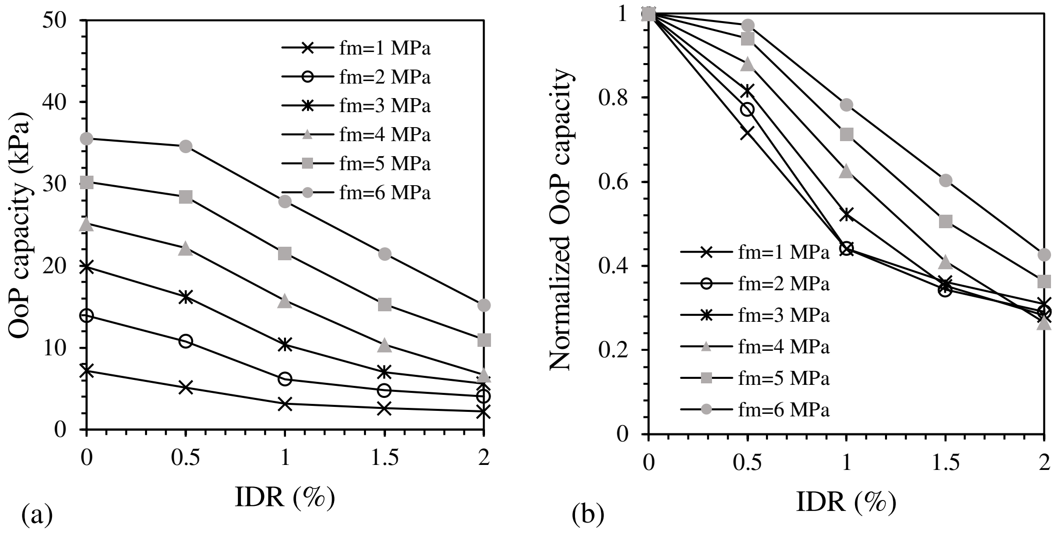

Fig 13. Decay of OoP capacity of infill walls vs IP drift - *l*=*h*=2600 mm, *t* = 200 mm (*h/t*=13) – (a); normalized OoP capacity (b).

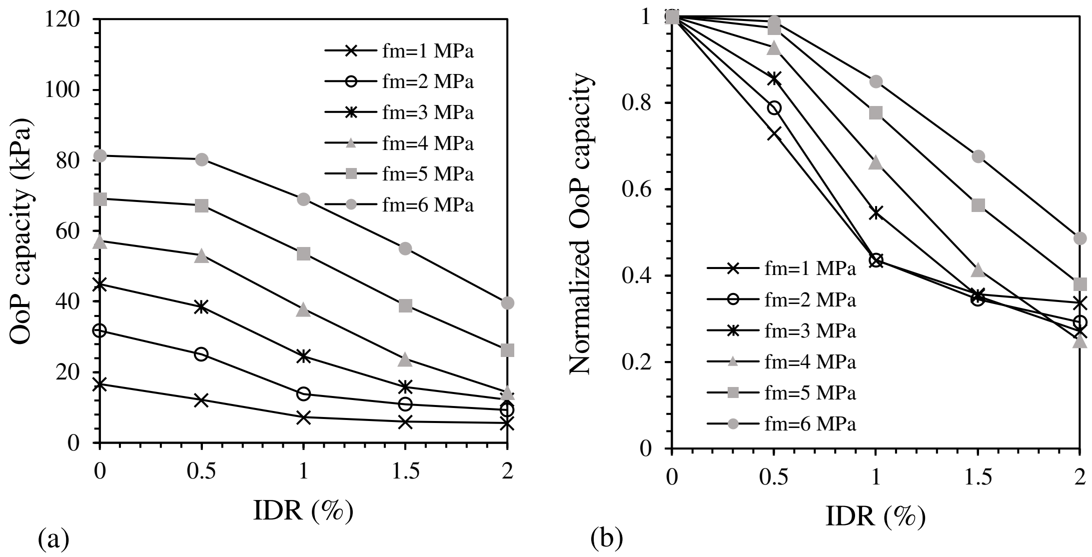

Fig 14. Decay of OoP capacity of infill walls vs IP drift - *l*=*h*=2600 mm, *t* = 300 mm (*h/t*=8.6) – (a); normalized OoP capacity (b).

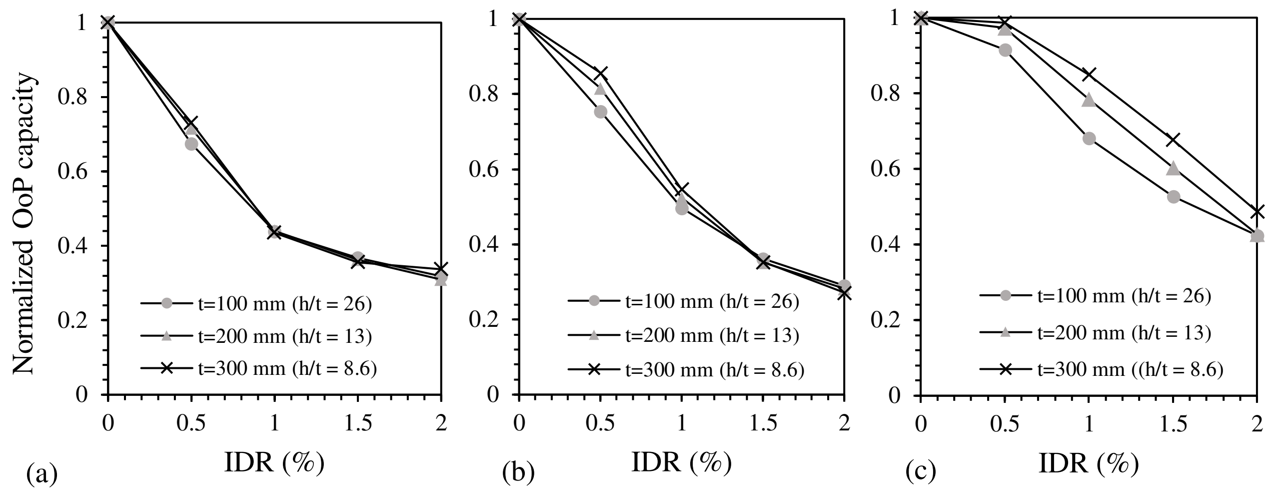

Fig 15. Comparison of decay of the OoP capacity of infill walls for *l*=*h*=2600 mm according to infill thickness (or slenderness ratio): a) f_m=1 MPa; b) f_m=3 MPa; c) f_m=6 MPa

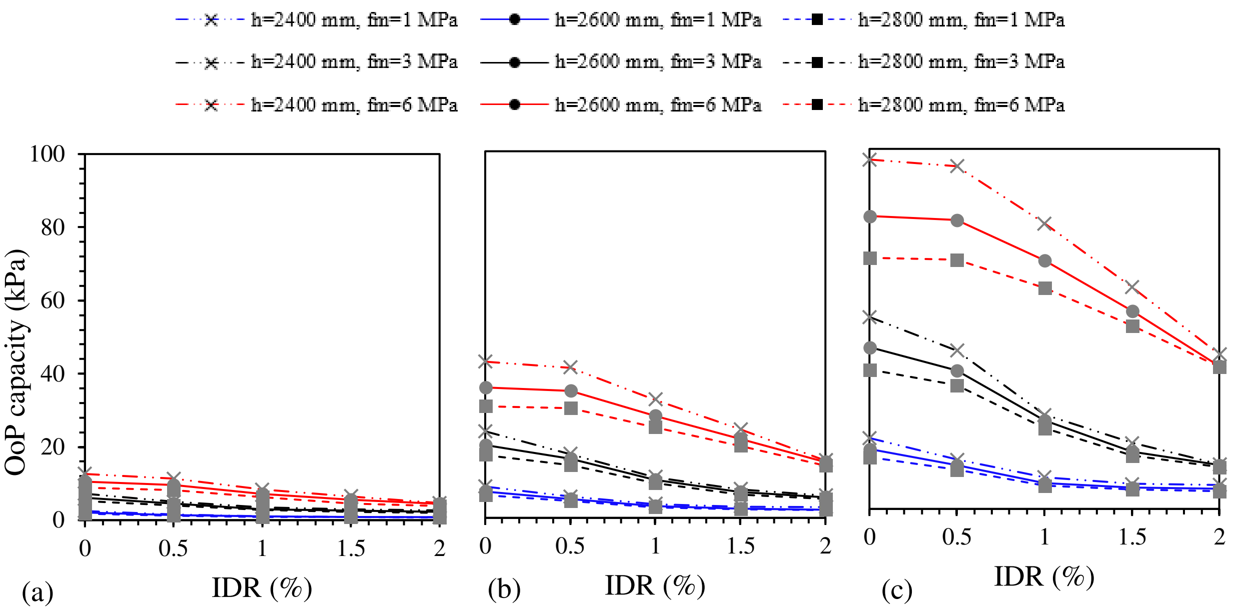

Fig 16. Comparative decay of OOP strength for infills of different size having aspect ratio 1: a) *t*=100 mm; b) *t*=200 mm; c) *t*=300 mm

Upon investigating the effect of aspect ratio on strength decay due to IP damage, it was found that it has a very little influence. It is different from what is shown by Wang et al. (2020), where they indicated a lesser reduction in OoP strength at the same level of IP damage when the aspect ratio was higher. As an example, a particular case of infill wall (height =2600 mm) for two different values of masonry strengths (1 and 6 MPa) is shown in Figs 17-19. Increase of aspect ratio slightly accelerated the strength decay process especially in the case of infill walls of higher slenderness (compare Fig.

17-b and Fig. 18-b) but the difference in the decay rate was negligible when the slenderness ratio was smaller (Fig 18-b & Fig 19-b).

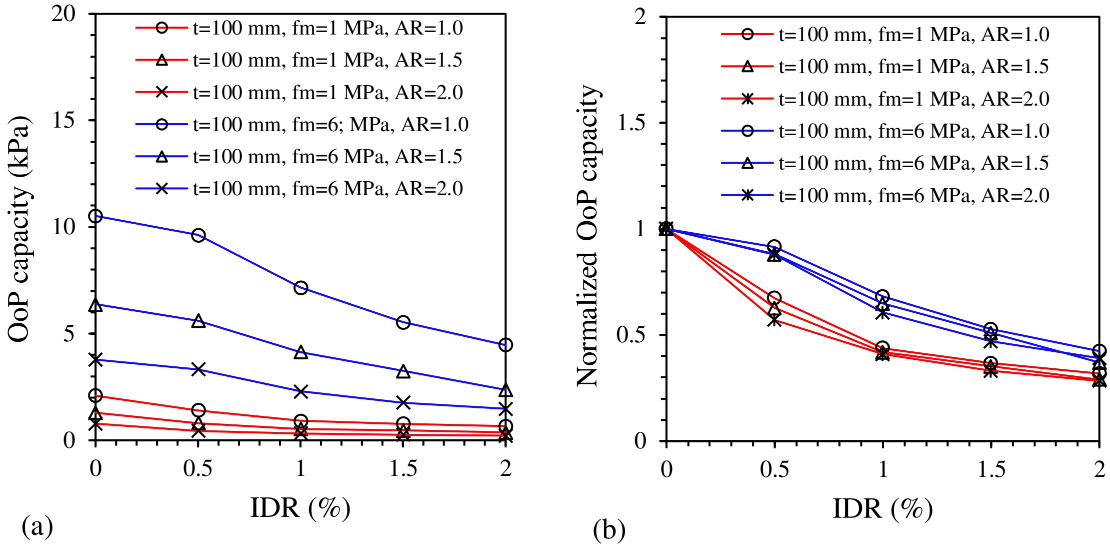

Fig 17. Decay of OoP capacity of infill walls vs IP damage according to the aspect ratio (AR) - *h*=2600 mm, *t* = 100 mm (h/t=26) (a); normalized OoP capacity (b).

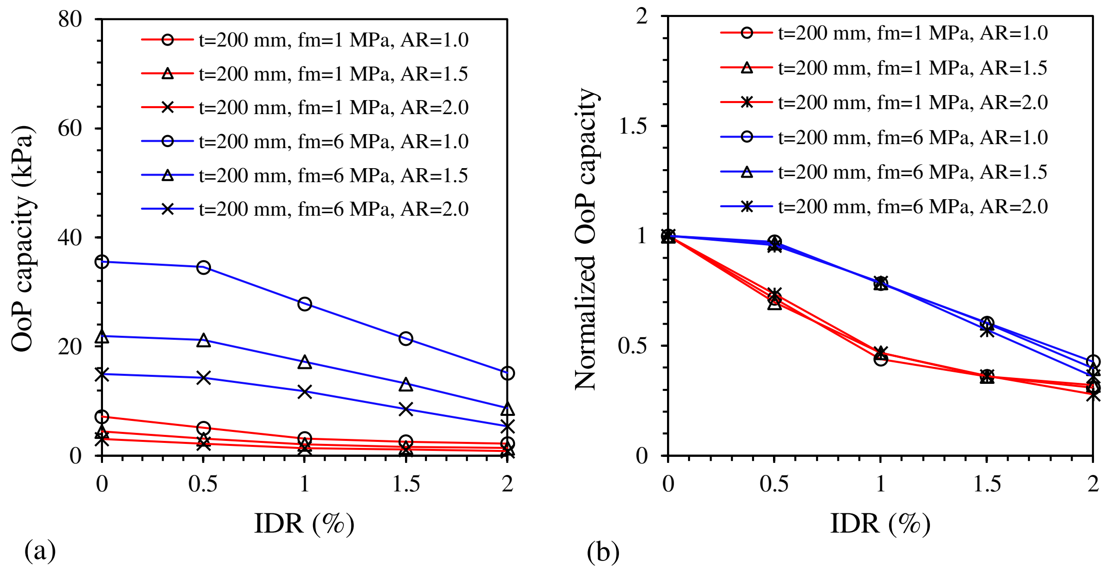

Fig 18. Decay of OoP capacity of infill walls vs IP damage according to the aspect ratio (AR) - *h*=2600 mm, *t* = 200 mm (h/t=13) (a); normalized OoP capacity (b).

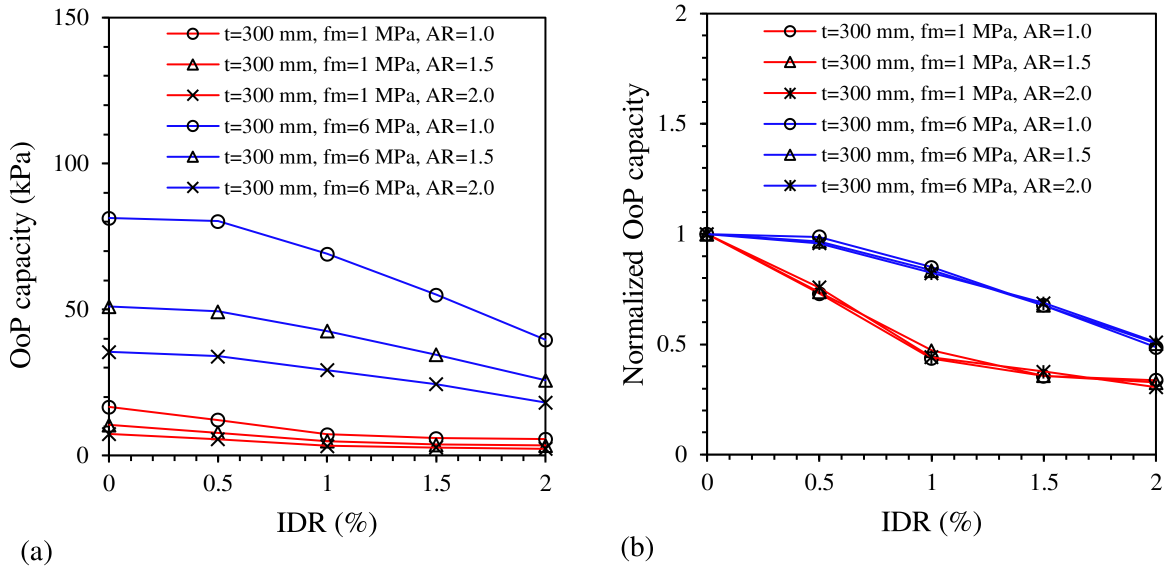

Fig 19. Decay of OoP capacity of infill walls vs IP damage according to the aspect ratio (AR) - *h*=2600 mm, *t* = 300 mm (h/t=8.6) – (a); normalized OoP capacity (b).

The complex nature of the OoP strength decay is easy to be understood from Fig 20 & 21. The reduction factors, numerically evaluated fixing the values of f_m and IDR for infills of different h/t ratios, are less scattered compared to the other ones calculated fixing the values of h/t and IDR for different values of f_m. This indicates that the large variation in OoP capacity of infills can be brought by differences in f_m.

Regarding the OoP stiffness, an initial stiffness was evaluated by estimating a secant stiffness using the point on the OoP load–displacement curves corresponding to one-third of the maximum strength as in Cavaleri et al. (2019). To calculate the decay of the stiffness, the OoP stiffness was evaluated after each increasing level of IP damage as shown in Fig 22. As in the case of the OoP strength, the numerical results showed the dependence of OoP stiffness decay on masonry strength and thickness (or h/t) of infills. But the decay of stiffness was not as scattered as the decay of strength. Some examples are shown in Figs 23-25, a case of infill of *h*=*l*=2600 mm. Unlike the strength, the OoP stiffness decays rapidly after the infill wall is damaged in IP by a small amount of drift. This is because the infill wall initially, after suffering IP damage, goes through a stiffness recovery process and gains the OoP strength peak at a larger displacement compared to the undamaged cases. The sensitivity of these parameters (f_m , h/t) on the decay of OoP stiffness becomes lesser when the infill is damaged in IP by a drift of more than 1%.

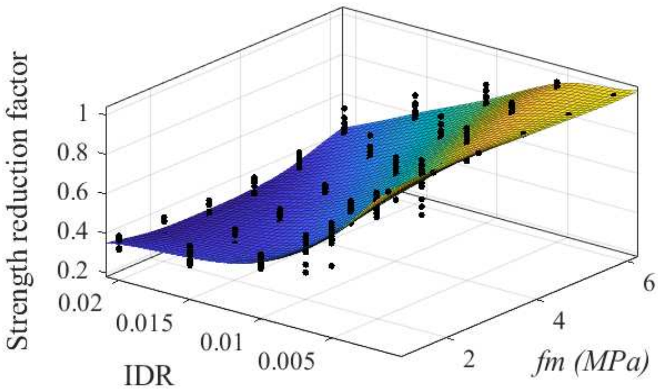

Fig 20. Strength reduction factor according to masonry strength and IP drift for various slenderness ratios

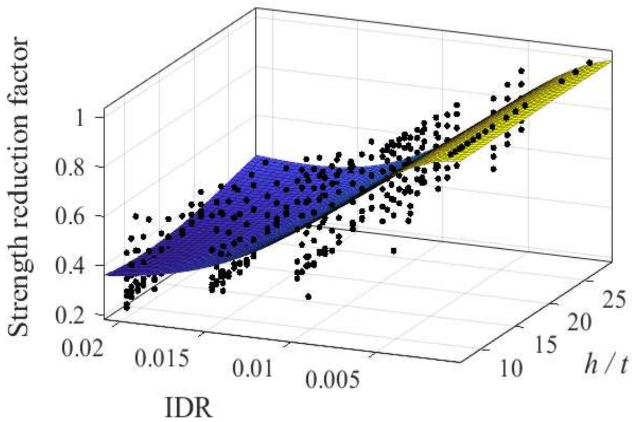

Fig 21. Strength reduction factor according to slenderness ratio and IP drift for various masonry strengths

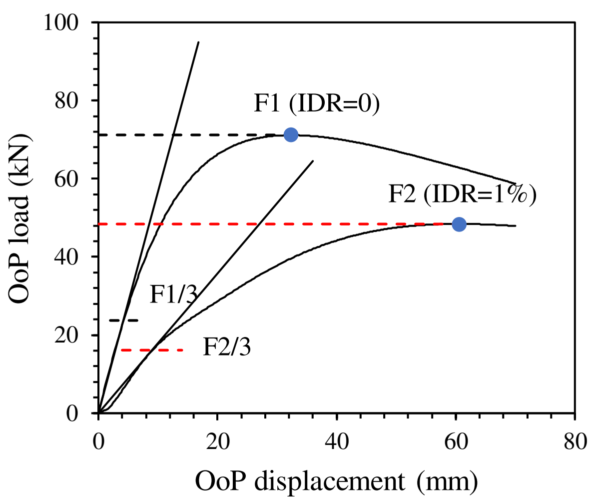

Fig 22. Example of evaluation of the OoP stiffness (infill with *l*=*h*=2600 mm, *t* = 100 mm, f_m=6 MPa)

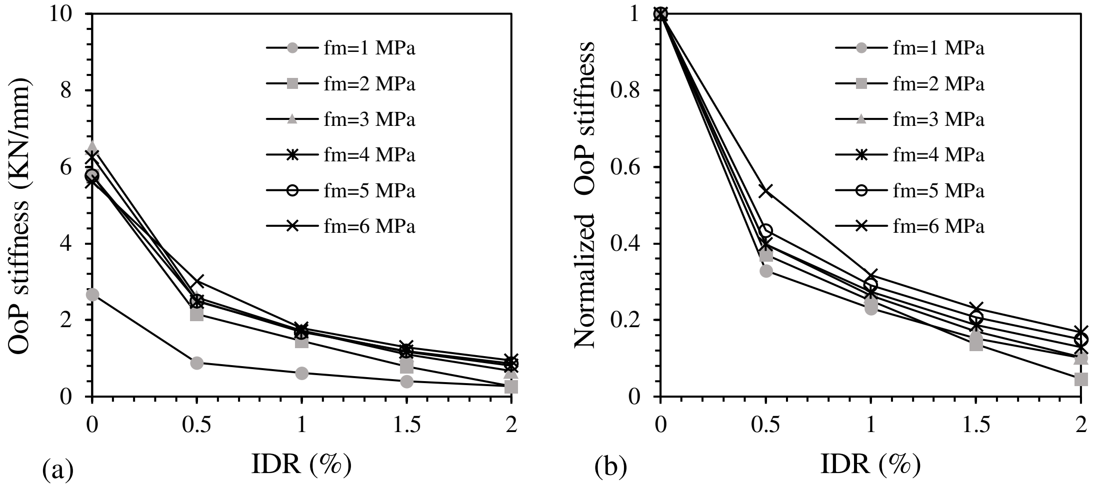

Fig 23. OoP stiffness decay - l=h=2600 mm, t = 100 mm (h/t=26) – (a); OoP normalized stiffness (b)

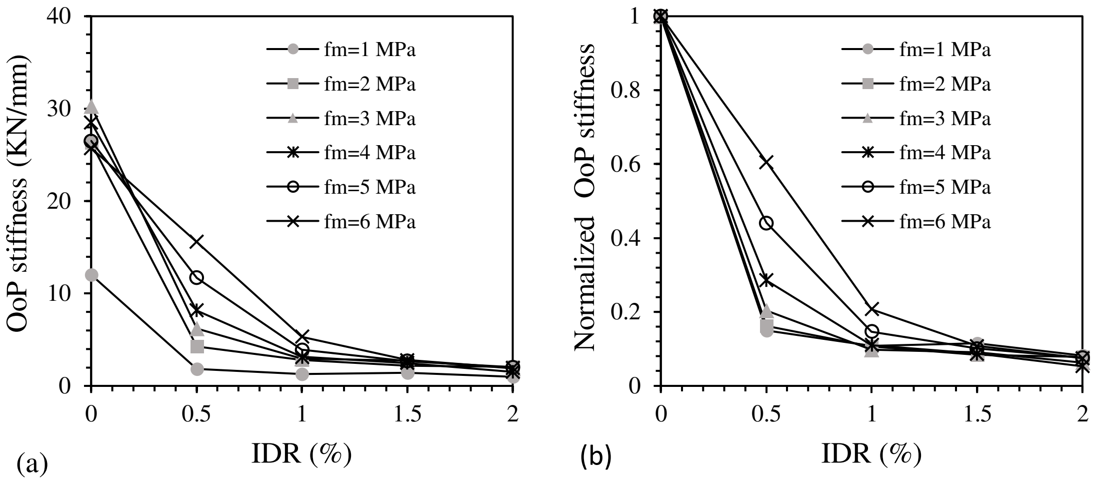

Fig 24. OoP stiffness decay - l=h=2600 mm, t = 200 mm (h/t=13) – (a); OoP normalized stiffness (b)

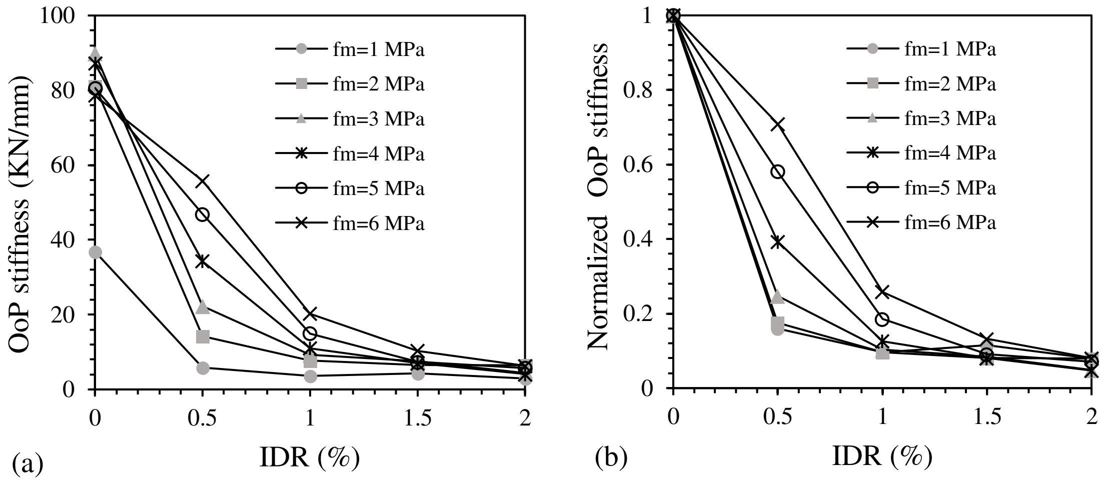

Fig 25. OoP stiffness decay - l=h=2600 mm, t = 300 mm (h/t=8.6) – (a); OoP normalized stiffness (b).

3.5 Influence of the frame stiffness

To study the impact of column stiffness, the column cross-section size was increased in both directions i.e. the direction contained in the infill plane and in the direction orthogonal to it. Upon increasing the stiffness, the OoP capacity of infill wall was slightly increased. Comparatively, the impact was higher when the dimension of columns contained in the infill plane was increased. Fig 26 shows the average increase in OOP capacity of the infill walls when columns' dimension was made higher than the reference column size, i.e. 300 mm × 300 mm (synthetically indicated as 300*300). The contribution of the columns' stiffness tends to decrease as the column's size gets larger i.e. it becomes less flexible. For example, the OoP strength of the 100 mm thick infill wall with compressive strength 6 MPa was increased by 1.19%, 1.71%, and 2.0%, when the column size was changed from 300mm×300 mm to 450mm×300 mm, 600mm×300 mm and 750mm×300 mm, respectively. The relative increase in the OoP capacity, with the increase in column size, was 1.19%, 0.52%, and 0.29%, respectively. This behaviour was similar for the 200 mm and 300 mm thick infill walls as shown in Fig 26 a-c. The higher stiffness of columns contributed more in the case of thicker infill walls, compared to thinner ones, and for the case of higher masonry strength. Nevertheless, the increase in capacity was not very significant. Such conclusion was also remarked by Liberatore et al. (2020) from their investigation.

In the current study, the flexural stiffness EI of the columns, corresponding to their minimum cross-sectional area 300×300 mm^2, for a concrete strength of 30 MPa and elastic modulus of 27500 MPa was 18.56×10^{12} Nmm^2. This minimum size of columns in case of masonry infilled RC frame buildings is defined by contemporary seismic codes, and from the current study, it was found sufficient for infill walls to gain full OoP strength. In this regard, Angel's (1994) and Abrams et al.'s (1996) recommendation for the stiffness of frames (EI = 25.83×10^{12} Nmm^2) appears as a sufficient requirement for the activation of arching effect in infill walls.

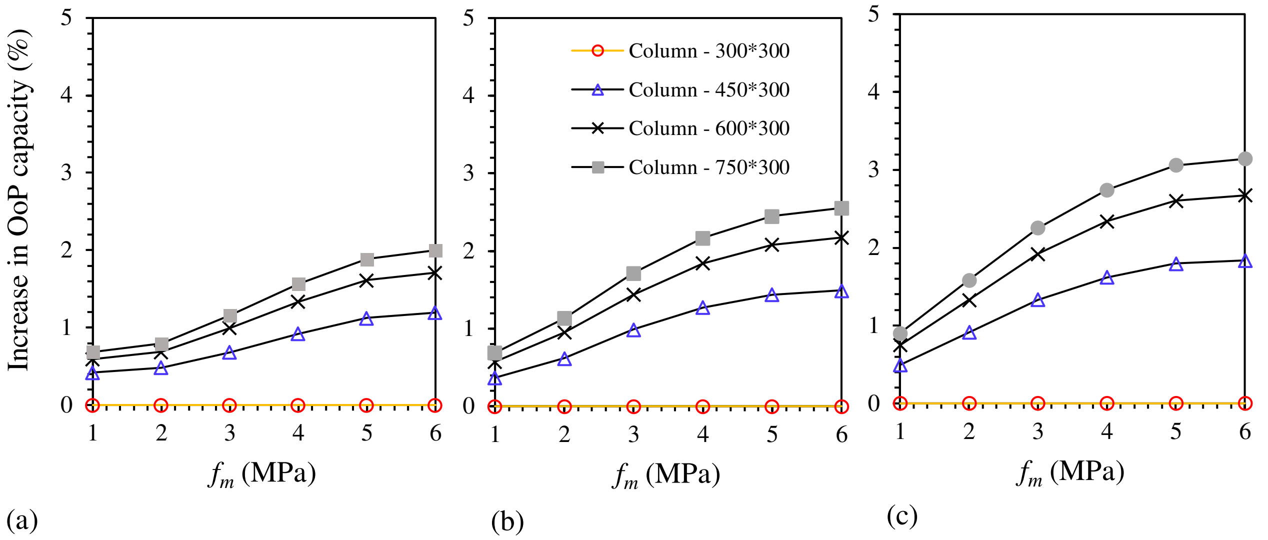

Fig 26. Increase in OoP capacity of infills according to the size of columns: a) t = 100 mm; b) t = 200 mm; c) t = 300 mm

4. Proposed empirical equations and validation

4.1 Case of IP undamaged infill walls

The masonry compressive strength and slenderness ratio significantly influence the OoP strength of infill walls. For an infill wall with an aspect ratio of 1, an equation to describe the OoP capacity (kPa) has been derived by fitting the numerical results, that is

$$q = 800 \frac{f_m^{\ 1.1}}{(h/t)^{1.9}} \qquad [5]$$

In the above equation, f_m has to be expressed in MPa. The correlation between the numerical results and the estimated OoP capacities as per Eq. 5 is shown in Fig 27-a. The dispersion of the numerical and estimated results is very low with a very high degree of the correlation coefficient (R^2 = 0.985). The average value of the ratio of estimated to numerical capacity was about 0.95 with the coefficient of variation (COV) as low as 15.1 percentage.

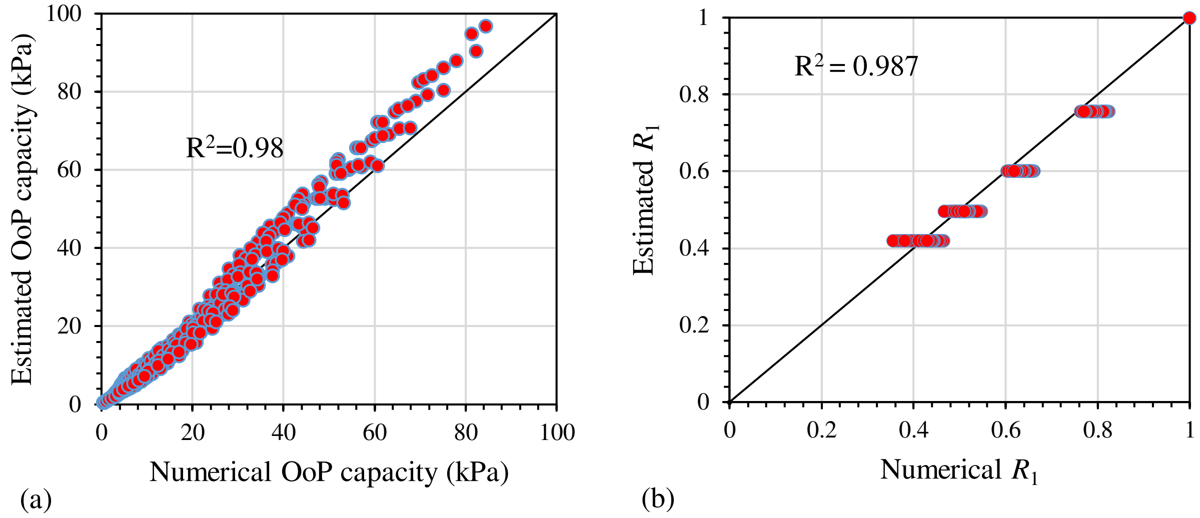

Fig 27. Scatter plot of the numerical and estimated quantities a) OoP capacity; b) reduction factor R_1

To consider the reduction of OoP capacity due to increase in the aspect ratio, an empirical equation to calculate the reduction factor R_1 was derived based on numerical results, that is

$$R_1 = (l/h)^{-1.25} \quad [6]$$

Eq. 6 is valid for the cases where $l \geq h$ and for infill walls bounded on all sides. The equation correlates the numerical data very well. The correlation between the numerical and the estimated values is shown in Fig 27-b. The strength reduction path represented by the Eq. 6, the numerical results, and some available experimental results are inserted in Fig 28.

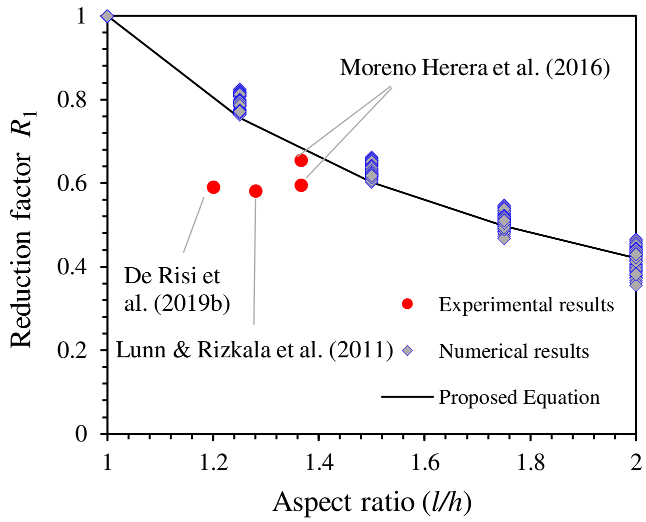

Fig 28. Comparison of the strength reduction factor according to the aspect ratio

Combining Eq. 5 and 6, a new equation (Eq. 7) can be formed to estimate the OoP capacity of infill walls, not IP-damaged previously. The equation is valid for infill walls bounded on four edges, for $l \geq h$ and f_m not larger than 11 MPa.

$$q = 800 \frac{{f_m}^{1.1}}{(h/t)^{1.9}} \times (l/h)^{-1.25} \qquad [7]$$

Eq. 7 has been checked with some experimental results (Table 4). Although the equation is solely derived from a regression analysis of the numerical results, it estimated OoP capacity with good accuracy (mean ratio 0.81, COV 30.5%). The correlation between the experimental and estimated capacity can also be observed from Fig 29.

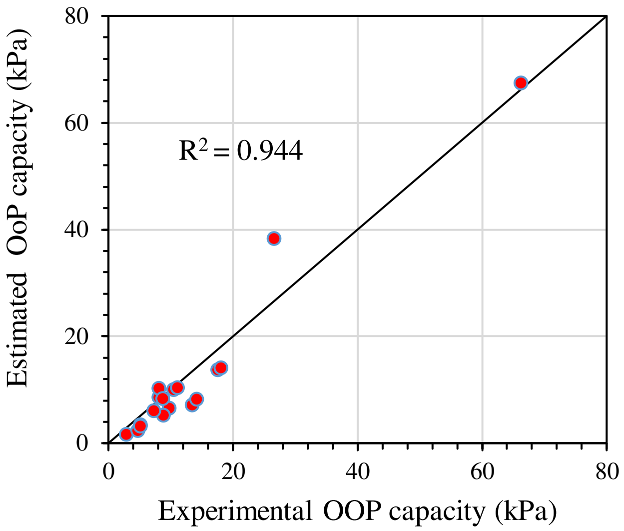

Fig 29. Scatter plot between the experimental and estimated OoP strength using Eq. 7

Table 4. Comparison of the experimental OoP strength and estimated strength using Eq. 7

Author	Specimen	Experimental Strength (kPa)	Estimated Strength (kPa)	$\frac{Estimated}{Experimental}$
Angel (1994)	1	8.18	8.64	1.06
Flanagan & Bennett (1999a)	18	26.60	38.33	1.44
	25	8.10	10.27	1.27
Calvi & Bolognini (2001)	10	2.92	1.71	0.59
Moreno-Herera et al. (2016)	W1	8.81	5.30	0.60
	W2	10.49	10.10	0.96
	W3	11.06	10.37	0.94
	W4	7.33	6.08	0.83
	W5	13.44	7.21	0.54
	W6	17.61	13.72	0.78
	W7	18.06	14.09	0.78
	W8	14.24	8.26	0.58
Spesdar (2017)	IF-ND	66.30	67.51	1.02
Furtado et al. (2018a)	M4	4.76	2.34	0.49
Ricci et al. (2018a)	80_OOP_4E	5.12	3.47	0.68
Ricci et al. (2018b)	120_OOP_4E	9.74	6.58	0.68
Di Domenico et al. (2018)	OOP_4E	5.12	3.27	0.64
De Risi et al. (2019b)	OOP	8.80	8.34	0.95
Di Domenico et al. (2019)	OOP_4E	9.74	6.58	0.68
mean				0.81
standard deviation				0.25
COV[%]				30.5

4.2 Case of previously IP damaged infill walls

From the discussion in section 3.4, it is clear that the amount of strength reduction due to IP damage is determined by the strength of masonry, slenderness ratio, level of IP drift and very less by the aspect ratio. The best curve fitting the numerical results yielded the following equations to determine the ratio of the damaged capacity P_{dam} to the undamaged capacity P_{undam}.

Based upon the level of IP damage and the strength of masonry, the strength reduction factor R_2 can be expressed as

$$R_2 = \frac{P_{dam}}{P_{undam}} = \min(0.5 \times f_m{}^{0.09} \times IDR^{-0.27}; 1) \quad [8]$$

Similarly, depending upon the level of IP damage and the slenderness ratio, the fitting equation of the following form was obtained.

$$R_2 = \frac{P_{dam}}{P_{undam}} = \min(0.69 \times \left(\frac{h}{t}\right)^{-0.08} \times IDR^{-0.27}; 1) \quad [9]$$

By integrating strength of masonry, slenderness ratio, and IP drift level (aspect ratio is ignored as it has the lowest impact), the strength reduction factor can be expressed as:

$$R_2 = \frac{P_{dam}}{P_{undam}} = \min(0.662 \times f_m^{\ 0.22} \times \left(\frac{h}{t}\right)^{-0.18} \times IDR^{-0.26};\ 1) \qquad [10]$$

In the above Eqs. 8-10, the IDR is expressed in percentage and f_m is in MPa. The factor R_2 takes the value 1 when IDR is equal to zero i.e. no IP damage. The correlation between the numerical results and estimated values by using Eqs. 8-10 can be seen in Fig 30.

Eq. 8 and Eq. 9 cover a small band of the numerical data relatively while Eq. 10 satisfy a wide range (Fig 31). The strength reduction factors estimated by using Eq. 10 for particular values of f_m and h/t for different levels of IDR are further shown in Fig 32. Moreover, the strength reduction factors estimated by the proposed equations and the strength reduction factors obtained by the experiments available in the literature are kept in Fig 33. Factor R_2 calculated according to Eq. 10 matches closely the variability shown by the experimental results (the related data are provided in Table 5).

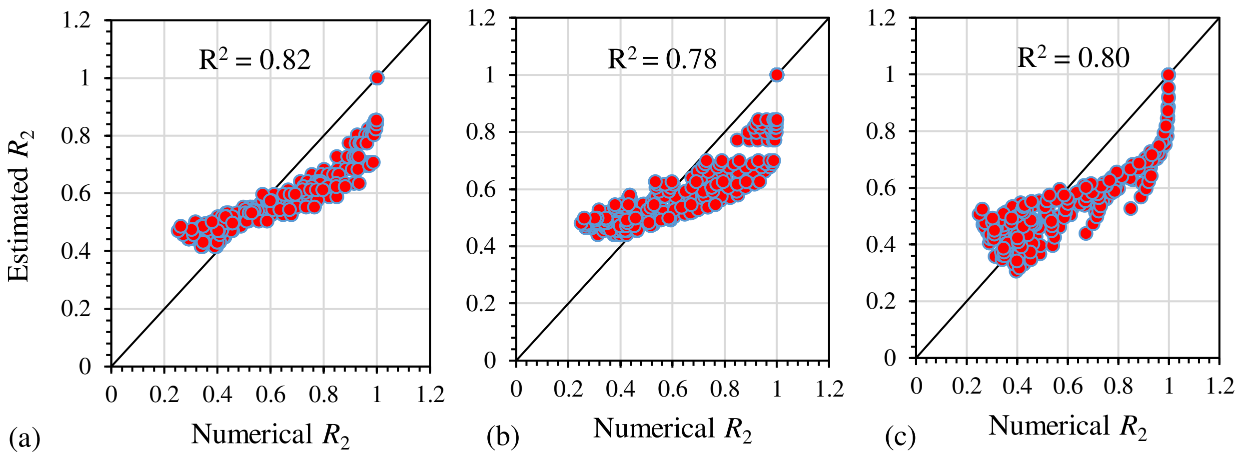

Fig 30. Scatter plot of the numerical and estimated values of the reduction factor R_2 using a) Eq. 8; b) Eq. 9; c) Eq. 10

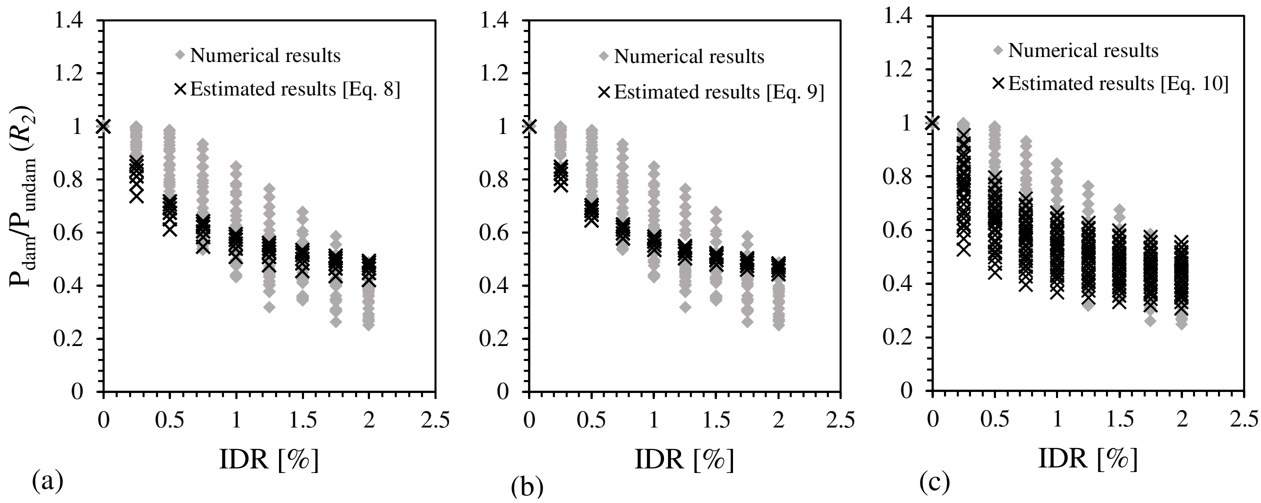

Fig 31. Comparison of the numerical and the estimated values of the reduction factor R_2: a) Eq.8; b) Eq. 9; c) Eq. 10

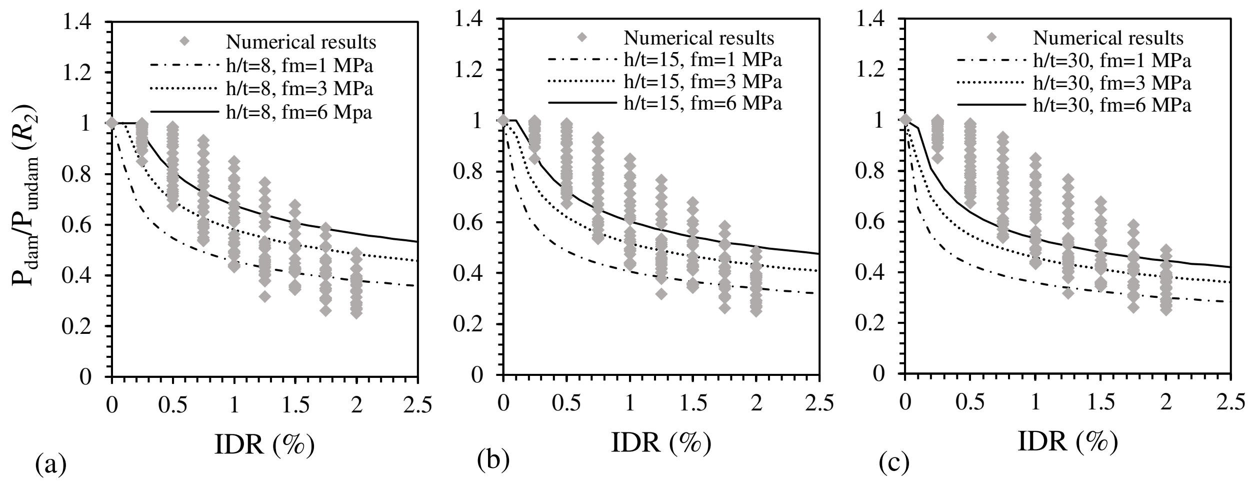

Fig 32. Comparison of the OoP strength numerical decay and the estimated decay by using Eq. 10: a) *h/t*=8; b) *h/t*=15; c) *h/t*=30

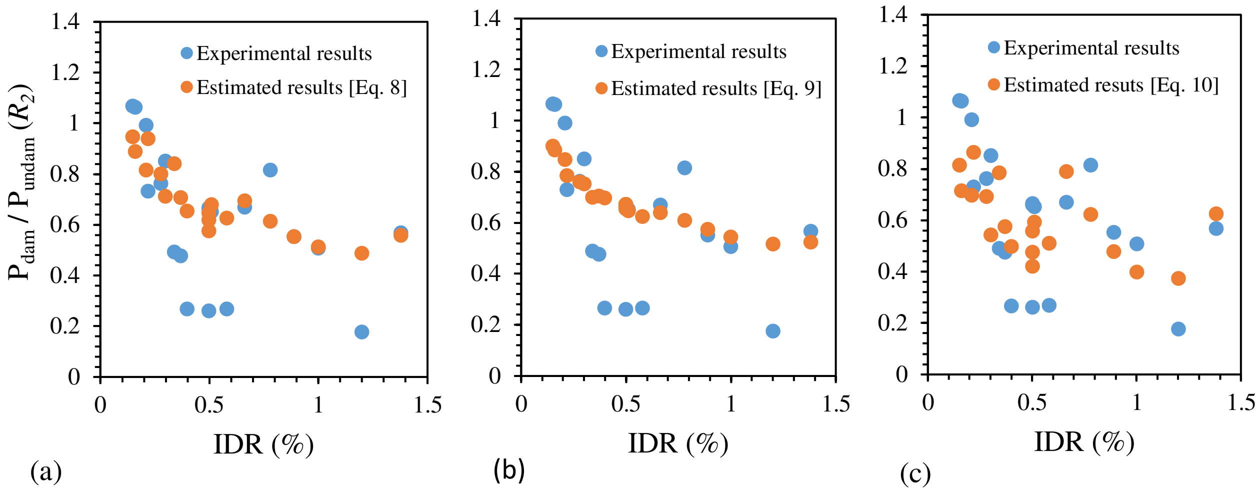

Fig 33. Comparison of the strength reduction factor obtained from experiments in the literature and those estimated by using the proposed Eq. 8 (a), Eq. 9 (b), Eq. 10 (c).

Table 5. Comparison of experimental and estimated [Eq.8 - Eq.11] values of P_{dam} / P_{undam}

Author	Specimen	$R_{Exp.}$	$R_{Est.}$ Eq. 8	$R_{Est.}$ Eq. 9	$R_{Est.}$ Eq. 10	$R_{Est.}$ Eq. 11	$\frac{Est.[Eq.8]}{Exp.}$	$\frac{Est.[Eq.9]}{Exp.}$	$\frac{Est.[Eq.10]}{Exp.}$	$\frac{Est.[Eq.11]}{Exp.}$
Angel (1994)	2	0.49	0.84	0.70	0.78	0.46	1.71	1.42	1.60	0.94
	3	0.73	0.94	0.79	0.87	0.63	1.28	1.08	1.18	0.87
Flanagan & Bennett (1999a)	19	0.82	0.61	0.61	0.62	0.86	0.75	0.75	0.76	1.06
Calvi & Bolognini (2001)	6	0.27	0.65	0.70	0.50	0.40	2.45	2.61	1.87	1.50
	2	0.18	0.49	0.52	0.38	0.18	2.73	2.91	2.11	1.02
Furtado et al. (2016)	Inf_03	0.26	0.58	0.67	0.42	0.57	2.21	2.58	1.62	2.18
Spesdar (2017)	IF-D1	0.67	0.69	0.64	0.79	0.86	1.04	0.96	1.18	1.29
Wang (2017)	IF_RC_ID	0.57	0.56	0.53	0.62	0.51	0.99	0.93	1.10	0.90
Ricci et al. (2018a)	OOP_L_80	1.06	0.89	0.89	0.72	1.00	0.83	0.83	0.67	0.94
	OOP_M_80	0.48	0.71	0.71	0.58	0.55	1.48	1.48	1.21	1.15
	OOP_H_80	0.27	0.63	0.63	0.51	0.40	2.34	2.33	1.91	1.48
Ricci et al. (2018b)	OOP_L_120	0.99	0.82	0.85	0.70	1.00	0.82	0.86	0.70	1.01
	OOP_M_120	0.67	0.65	0.67	0.56	0.80	0.97	1.01	0.84	1.20
	OOP_H_120	0.55	0.55	0.58	0.48	0.53	1.00	1.04	0.87	0.95
Akhoundi et al. (2018)	SIF-0.3%-B	0.85	0.71	0.75	0.54	0.52	0.83	0.89	0.64	0.61
	SIF-0.5%-B	0.66	0.62	0.66	0.48	0.36	0.94	0.99	0.72	0.54
	SIF-1.0%-B	0.51	0.51	0.54	0.40	0.22	1.01	1.07	0.78	0.43
De Risi et al. (2019b)	OOP_L_80	1.07	0.95	0.90	0.81	1.00	0.89	0.84	0.76	0.94
	OOP_M_80	0.76	0.80	0.76	0.69	0.84	1.05	1.00	0.91	1.10
	OOP_H_80	0.65	0.68	0.65	0.59	0.55	1.04	0.99	0.91	0.84
Mean							1.32	1.33	1.12	1.05
Standard deviation							0.60	0.67	0.45	0.37
COV [%]							46%	50%	40%	35.36%

Note: Est.-estimated by equations, Exp. –experimental values

For further comparisons, strength reduction factors calculated from few recent proposals available in the literature (Furtado et al. 2018b; Ricci et al. 2018a; and Cavaleri et al. 2019) are also kept in Fig 34. The proposal of Furtado et al. (2018b) and Ricci et al. (2018a) give similar results as both equations were proposed based on the same test results. Additionally, results obtained from a new model by Di Domenico et al. (2021) [Eq. 11] including the effect of aspect ratio in the strength decay is shown in Fig 34-b. The before mentioned model for the reduction factor is expressed as

$$R = \frac{P_{dam}}{P_{undam}} = \min\left\{1; \left(1.438 - 0.245\frac{l}{h} - 0.042 \times \min\left(\frac{h}{t}; 20.4\right)\right) \times IDR^{-0.719}\right\} \qquad [11]$$

The calculated strength factors from this equation as well are kept in Table 5.

Relatively, Eq. 11 by Di Domenico et al. (2021) has a better prediction since the equation itself was derived from the regression analysis of experimental results included in Table 5 (except Flanagan and Bennett 1999b; Furtado et al. 2016; Spesdar 2017; Wang 2017; Akhoundi et al. 2018). Nevertheless, considering that the proposed equation (Eq. 10) was derived based on the numerical results alone, it is equally effective. It has to be remembered that the proposed Eq. 10 considers the masonry strength while Eq. 11 does not consider it.

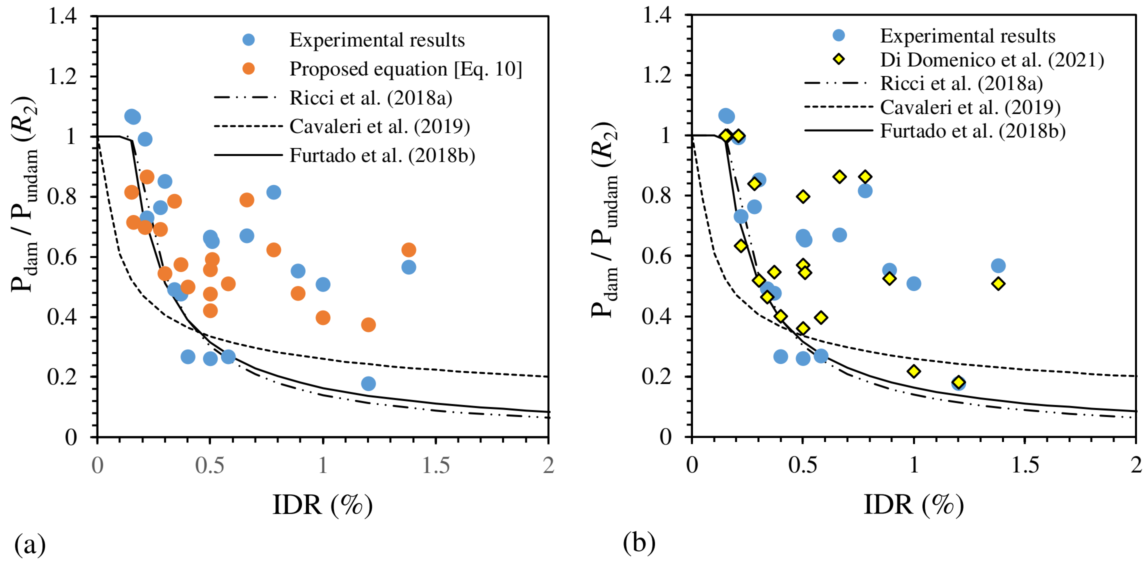

Fig 34. Comparison of OoP capacity decay from experimental results, numerical results and some available proposals: a) focusing on proposed equation; b) focusing of proposals of Di Domenico et al. (2021)

It has not to be forgotten that the experimented infills have variations also in loadings besides the variations in geometrical (h/t, l/h) and mechanical (f_m, E_m) properties. Some specimens were subjected to monotonic load in IP and OoP directions while others were subjected to cyclic or half cyclic loads. This has an impact on the level of strength reduction which makes not possible a true comparison among these experimental results. Nevertheless, all test results help to show the variability and the uncertainties in OoP strength decay due to IP damage.

Finally, considering the strength reduction factor R_2 due to IP damage from Eq. 10, a new equation (Eq. 12) is proposed to estimate the OoP capacity of the URM infills in IP-damaged conditions, that is

$$q = 800\frac{f_m^{\ 1.1}}{(h/t)^{1.9}} \times \left(l/h\right)^{-1.25} \times \min(0.662 \times f_m^{\ 0.22} \times \left(\frac{h}{t}\right)^{-0.18} \times IDR^{-0.26};\ 1) \qquad [12]$$

The comparison between the estimated capacities (using Eq. 12) and experimental results shows good agreement with the mean of ratio 0.9 and COV equal to 31.6% (Table 6). The proposed equation facilitates the calculation and comparison of OoP strength with those experimental tests where reference undamaged specimens are unavailable like in Da Porto et al. (2013), Hak et al. (2014) as shown in Table 6. The correlation between the estimated and test results can also be observed from Fig 35.

Table 6. Comparison of the experimental and estimated OOP strengths for IP damaged infills

Author	Specimen	Experimental Strength (kPa)	Estimated Strength (kPa)	$\frac{Estimated}{Experimental}$
Angel (1994)	2b	4.02	6.35	1.58
	3b	5.98	6.50	1.09
	6b	12.39	9.99	0.81
Calvi & Bolognini (2001)	2	0.52	0.64	1.24
	6	0.78	0.86	1.10
Pereira et al. (2011)	Wall_REF_01	2.07	1.98	0.96
Da Porto et al. (2013)	URM_U	18.46	11.36	0.62
Hak et al. (2014)	TA1	13.54	10.48	0.77
	TA2	8.25	9.18	1.11
	TA3	13.17	11.65	0.88
Spesdar R. (2017)	IF-D1	44.40	55.75	1.26
Wang C. (2017)	IF-RC-ID	37.60	34.88	0.93
Ricci et al. (2018b)	80_IP+OOP_L	5.44	2.48	0.46
	80_IP+OOP_M	2.44	2.00	0.82
	80_IP+OOP_H	1.37	1.78	1.29
Ricci et al. (2018b)	120_IP+OOP_L	9.67	4.60	0.48
	120_IP+OOP_M	6.49	3.67	0.57
	120_IP+OOP_H	5.37	3.16	0.59
De Risi et al. (2019b)	IP_L-OOP	9.39	6.79	0.72
	IP_M-OOP	6.72	5.77	0.86
	IP_H-OOP	5.74	4.94	0.86
mean				0.9
Standard deviation				0.29
COV [%]				31.6

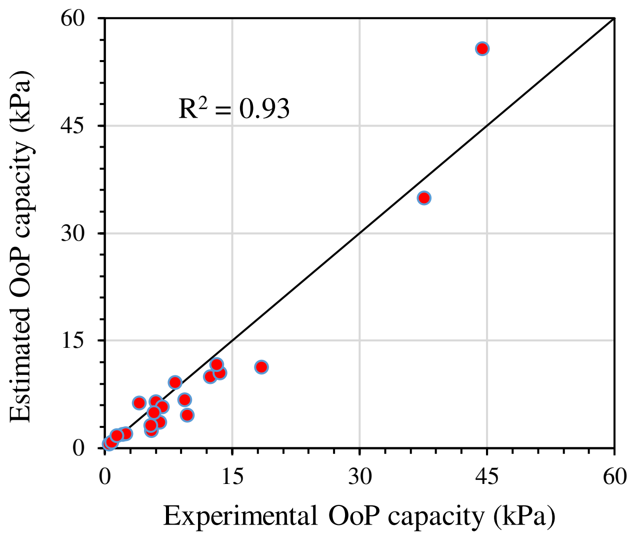

Fig 35. Scatter plot between the experimental OoP strength and estimated strength by using Eq. 12 for IP damaged specimens

Additionally, a best fitting equation to determine the residual initial stiffness factor $K_{r,ini}$ expressed as a ratio of damaged stiffness $K_{ini,dam}$ to undamaged stiffness $K_{ini,undam}$ has been formed by considering the reduction only due to IP drift as:

$$K_{r,ini} = \frac{K_{ini,dam}}{K_{ini,undam}} = \min(0.17 \times IDR^{-0.8};\ 1) \qquad [13]$$

Eq. 13 is similar to the one proposed by Cavaleri et al. (2019) as shown in Fig 36-a. In the same figure, the models proposed by Furtado et al. (2018b) and Ricci et al. (2018a) for the reduction of the secant stiffness, corresponding to the first infill wall macro-cracking, are also included for comparison. It has to be noted that it is complex to identify the value of the force and the displacement corresponding to the first macro-cracking during experiments. Furtado et al. (2018b) and Ricci et al. (2018a) assumed a point in the load-displacement curve where significant yielding started. Stiffness evaluated with these approaches cannot be compared directly to one adopted in this study. But since the idea is to recognize the decay of OoP stiffness, the comparison serves the purpose.

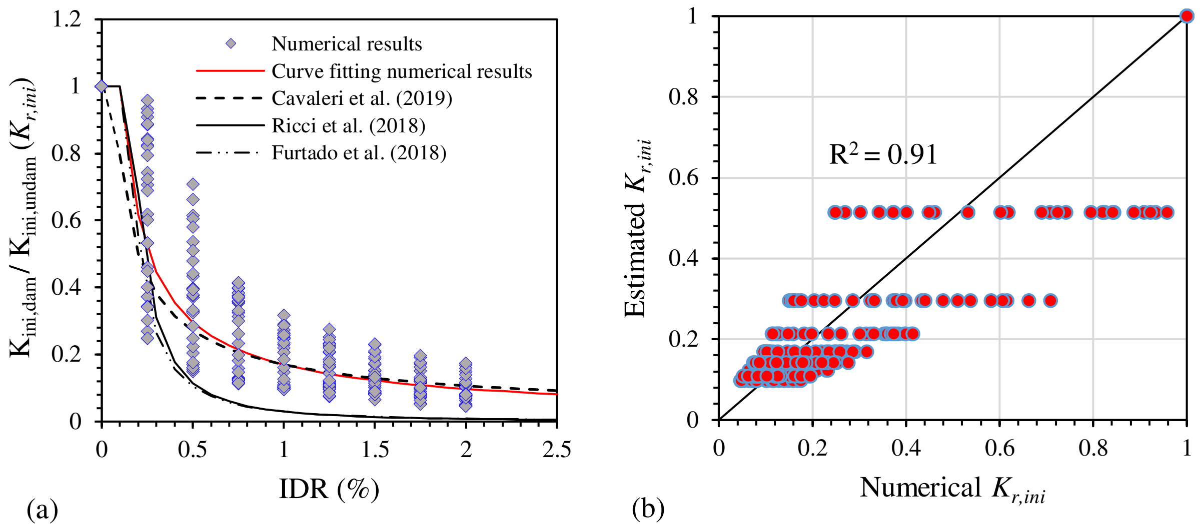

Fig 36. a) Decay of initial OoP stiffness b) Scatter plot between the numerical and estimated (using Eq. 13) stiffness decay ratio

5. Conclusions

In the parametric study conducted, the OoP capacity of URM infill walls bounded by frames on all sides has been investigated in detail. Numerical analyses were carried out by using a recently proposed macro-element model which is able to consider both IP and OoP response of infills. In evaluating the capacities, different parameters were investigated such as the masonry strength f_m, slenderness ratio (*h/t*), aspect ratio (*l/h*), previous IP damage, and stiffness of the bounding frames.

The OoP capacity of URM infill walls was found to be heavily dependent on masonry strength and infill wall thickness (or slenderness ratio). The OoP strength was proportional to masonry strength and decreasing when the slenderness ratio and the aspect ratio increased. For any infill wall, the OoP strength was found to be significantly reduced when infill slenderness ratio was greater than 20 (EC8 limits it to 15). Similarly, the OoP strength decreased by almost 60% when doubling the aspect ratio (i.e. length two times the height). The reduction of OoP capacity due to the increasing slenderness or aspect ratio was not affected by the compressive strength of masonry infills.

The OoP strength decay due to prior IP damage was affected by masonry strength and thickness (or the slenderness ratio) of infill walls. The decay of OoP strength was lower when the infill walls were thicker (lower slenderness ratio) and when the masonry was stronger (higher compressive strength).

The OoP strength decay was less influenced by the aspect ratio of infill walls. Likewise, the OoP stiffness decay was also found to be affected by the masonry strength and the slenderness ratio of infill walls. However, the scattering of the numerical results was lower as compared to the case of OoP strength.

Based on the numerical results, empirical equations have been proposed to determine the OoP strength of the previously IP-damaged or undamaged infill wall, respectively. To evaluate the decay of the OoP strength due to previous IP damage, the proposed equation considering the influence of masonry strength and slenderness ratio in addition to IP drift level showed more affinity with the experimental findings compared to other equations which integrate only the effect of IP drift level and masonry strength or IP drift level and slenderness ratio. The proposed equations provide reliable results when compared with experimental results in both, IP-damaged or undamaged cases, respectively, also indicating the efficiency of the adopted macro-element model to capture the OoP capacity of infill walls.

The OoP strength of infill walls is also influenced by the stiffness of the surrounding frames. However, a stiffness higher than that required increase the OoP strength of infill walls in a not significative way. A column cross-sectional size of 300 mm × 300 mm, which is a minimum requirement in RC frames, as recommended by the contemporary seismic building codes, was found to be sufficient for the activation of the full OoP strength in infill walls.

Data Availability Statement

All data, models, and code generated or used during the study appear in the submitted article.

Acknowledgements

This research has been carried out using the resources of ReLUIS (The Laboratories University Network of seismic engineering, Italy) and the support is gratefully acknowledged.

References

Abrams, D., Angel, R., and Uzarski, J. (1996). "Out-of-plane strength of unreinforced masonry infills." Earthquake Spectra, 12(4), 825–44.

Agnihotri, P., Singhal, V., and Rai, D. C. (2013). "Effect of in-plane damage on out-of-plane strength of unreinforced masonry walls." *Engineering Structures*, 57, 1–11.

Akhoundi, F., Vasconcelos, G., and Lourenço, P. (2018). "Experimental Out-Of-Plane Behavior of Brick Masonry Infilled Frames." International Journal of Architectural Heritage, 14(2), 221–237.

Angel, R. (1994). "Behavior of reinforced concrete frames with masonry infills." PhD, University of Illinois at Urbana-Champaign, Illinois.

Anić, F., Penava, D., Abrahamczyk, L., and Sarhosis, V. (2020). "A review of experimental and analytical studies on the out-of-plane behaviour of masonry infilled frames." Bulletin of Earthquake Engineering, 18(5), 2191–2246.

Braga, F., Manfredi, V., Masi, A., Salvatori, A., and Vona, M. (2011). "Performance of non-structural elements in RC buildings during the L'Aquila, 2009 earthquake." Bulletin of Earthquake Engineering, 9(1), 307–324.

Butenweg, C., Marinković, M., and Salatić, R. (2019). "Experimental results of reinforced concrete frames with masonry infills under combined quasi-static in-plane and out-of-plane seismic loading." Bulletin of Earthquake Engineering, 17(6), 3397–3422.

Calvi, G. M., and Bolognini, D. (2001). "Seismic response of reinforced concrete frames infilled with weakly reinforced masonry panels." Journal of Earthquake Engineering, 5(2), 153–185.

Castaldo, P., Gino, D., Bertagnoli, G., and Mancini, G. (2020). "Resistance model uncertainty in non-linear finite element analyses of cyclically loaded reinforced concrete systems." Engineering Structures, 211, 110496.

Castaldo, P., Gino, D., and Mancini, G. (2019). “Safety formats for non-linear finite element analysis of reinforced concrete structures_ discussion, comparison and proposals.” Engineering Structures, 18.

Castaldo, P., Tubaldi, E., Selvi, F., and Gioiella, L. (2021). “Seismic performance of an existing RC structure retrofitted with buckling restrained braces.” Journal of Building Engineering, 33, 101688.

Cavaleri, L., Zizzo, M., and Asteris, P. G. (2019). “Residual out-of-plane capacity of infills damaged by in-plane cyclic loads.” Engineering Structures, 109957.

Celarec, D., and Dolšek, M. (2013). “The impact of modelling uncertainties on the seismic performance assessment of reinforced concrete frame buildings.” Engineering Structures, 52, 340–354.

Dawe, J. L., and Seah, C. K. (1989). “Out-of-plane resistance of concrete masonry infilled panels.” Canadian Journal of Civil Engineering, 16(6), 854–864.

De Luca, F., Verderame, G. M., Gómez-Martínez, F., and Pérez-García, A. (2013). “The structural role played by masonry infills on RC building performances after the 2011 Lorca, Spain, earthquake.” Bulletin of Earthquake Engineering, 12(5), 1999–2026.

De Risi, M. T., Di Domenico, M., Ricci, P., Verderame, G. M., and Manfredi, G. (2019b). “Experimental investigation on the influence of the aspect ratio on the in-plane/out-of-plane interaction for masonry infills in RC frames.” Engineering Structures, 189, 523–540.

De Risi, M., Del Gaudio, C., and Verderame, G. (2019a). “Evaluation of Repair Costs for Masonry Infills in RC Buildings from Observed Damage Data: the Case-Study of the 2009 L’Aquila Earthquake.” Buildings, 9(5), 122.

Decanini, L. D., De Sortis, A., Goretti, A., Liberatore, L., Mollaioli, F., and Bazzurro, P. (2004). “Performance of Reinforced Concrete Buildings during the 2002 Molise, Italy, Earthquake.”

Earthquake Spectra, 20(1_suppl), 221–255.Del Vecchio, C., Di Ludovico, M., Pampanin, S., and Prota, A. (2018). “Repair Costs of Existing RC Buildings Damaged by the L’Aquila Earthquake and Comparison with FEMA P-58 Predictions.” Earthquake Spectra, 34(1), 237–263.

Di Domenico, M., De Risi, M. T., Ricci, P., Verderame, G. M., and Manfredi, G. (2021). “Empirical prediction of the in-plane/out-of-plane interaction effects in clay brick unreinforced masonry infill walls.” Engineering Structures, 227, 111438.

Di Domenico, M., Ricci, P., and Verderame, G. M. (2018). “Experimental Assessment of the Influence of Boundary Conditions on the Out-of-Plane Response of Unreinforced Masonry Infill Walls.” Journal of Earthquake Engineering, 24(6), 881–919.

Di Domenico, M., Ricci, P., and Verderame, G. M. (2019). “Predicting the Out-Of-Plane Seismic Strength of Unreinforced Masonry Infill Walls”. Journal of Earthquake Engineering, 1–38.

Di Domenico, M., Ricci, P., and Verderame, G. M. (2019). “Experimental assessment of the out-of-plane strength of URM infill walls with different slenderness and boundary conditions.” Bulletin of Earthquake Engineering, 17(7), 3959–3993.

Di Trapani, F., G. Macaluso, L. Cavaleri, and M. Papia. (2015). “Masonry infills and RC frames interaction: Literature overview and state of the art of macromodeling approach.” European Journal of Environmental and Civil Engineering, 19 (9), 1059–1095.

Di Trapani, F., Bertagnoli, G., Ferrotto, M.F., Gino, D. (2018). “Empirical equations for the direct definition of stress-strain laws for fiber-section-based macromodeling of infilled frames.” Journal of Engineering Mechanics ASCE, 144(11), 04018101.

Donà, M., Minotto, M., Bernardi, E., Saler, E., Verlato, N., and da Porto, F. (2019). “Macro-modelling of combined in-plane and out-of-plane seismic response of thin strengthened masonry infills.” Proceedings of the 7th International Conference on Computational Methods in Structural Dynamics and Earthquake Engineering (COMPDYN 2019), Institute of Structural Analysis and

Antiseismic Research School of Civil Engineering National Technical University of Athens (NTUA) Greece, Crete, Greece, 2449–2463.110.

Donà, M., Minotto, M., Bernardi, E., Saler, E., Verlato, N., and da Porto, F. (2019). "Macro-modelling of combined in-plane and out-of-plane seismic response of thin strengthened masonry infills." Proceedings of the 7th International Conference on Computational Methods in Structural Dynamics and Earthquake Engineering (COMPDYN 2019), Institute of Structural Analysis and Antiseismic Research School of Civil Engineering National Technical University of Athens (NTUA) Greece, Crete, Greece, 2449–2463.

Flanagan, R. D., and Bennett, R. M. (1999a). "Bidirectional Behavior of Structural Clay Tile Infilled Frames." Journal of Structural Engineering, 125(3), 236–244.

Flanagan, R. D., and Bennett, R. M. (1999b). "Arching of Masonry Infilled Frames: Comparison of Analytical Methods." Practice Periodical on Structural Design and Construction, 4(3), 105–110.

Furtado, A., Rodrigues, H., Arêde, A., and Varum, H. (2016). "Experimental evaluation of out-of-plane capacity of masonry infill walls." Engineering Structures, 111, 48–63.

Furtado, A., Rodrigues, H., Arêde, A., and Varum, H. (2018a). "Effect of the Panel Width Support and Columns Axial Load on the Infill Masonry Walls Out-Of-Plane Behavior." Journal of Earthquake Engineering, 24(4), 653–681.

Furtado, A., Rodrigues, H., Arêde, A., and Varum, H. (2018b). "Out-of-plane behavior of masonry infilled RC frames based on the experimental tests available: A systematic review." Construction and Building Materials, 168, 831–848.

Hak, S., Morandi, P., and Magenes, G. (2014). "Out-of-plane experimental response of strong masonry infills." 2nd European conference on earthquake engineering and seismology, 12.

Holický, M., Retief, J. V., and Sýkora, M. (2016). “Assessment of model uncertainties for structural resistance.” Probabilistic Engineering Mechanics, 45, 188–197.

Holmes, M. (1961). “Steel Frames with Brickwork and Concrete Infilling”, in: Proceedings of the Institution of Civil Engineers. pp. 473 ‑ 478.

Liauw, T.C., Kwan, K.H., 1984. Nonlinear Behaviour of Non-Integral Infilled Frames. Computers & Structures 18, 551 ‑ 560.

Liberatore, L., AlShawa, O., Marson, C., Pasca, M., and Sorrentino, L. (2020). “Out-of-plane capacity equations for masonry infill walls accounting for openings and boundary conditions.” Engineering Structures, 207, 110198.

Longo, F., Wiebe, L., da Porto, F., and Modena, C. (2016). “Seismic response history analysis including out-of-plane collapse of unreinforced masonry infill walls in RC frame structures.” 16th International Brick and Block Masonry Conference, CRC Press, Padova.

Lunn, D. S., and Rizkalla, S. H. (2011). “Strengthening of Infill Masonry Walls with FRP Materials.” Journal of Composites for Construction, 15(2), 206–214.

Mainstone, R.J. (1974). “Supplementary Note on the Stiffness and Strengths of Infilled Frames.” Presented at the Building Research Station, Garston, UK.

Mainstone, R.J. (1971). “On The Stiffness and Strength of Infilled Frames.” in: Proceedings of the Institution of Civil Engineers. pp. 57 ‑ 90.

Mander, J.B., Priestley, M.J.N., and Park, R (1988). “Theoretical stress-strain model for confined concrete.” Journal of structural engineering, 114(8),1804–26.

McDowell, E.L., K.E. McKee K.E., and Sevin E. (1956b). “Discussion of arching action theory of masonry walls.” Proceedings of the American Society of Civil Engineers, Journal Structural Division. 1067/27-40.

McDowell, E.L., K.E. McKee, and E. Sevin E. (1956 a). “Arching action theory of masonry walls.” Proceedings of the American Society of Civil Engineers, Journal Structural Division. 82(ST2), 915/1–915/18.

McKenna, F., Fenves, G.L., and Scott, M.H. (2000). “Open system for earthquake engineering simulation.” University of California, Berkeley, CA.

Menegotto, M., and P. E. Pinto. (1973). “Method of analysis for cyclically loaded RC plane fames including changes in geometry and non-elastic behavior of elements under combined normal force and bending.” In Proc., IABSE Symp. on the Resistance and Ultimate Deformability of Structures Acted on by Well Defined Repeated Loads, 15–22. Zürich, Switzerland: International Association for Bridge and Structural Engineering.

Moghadam, H., and Goudarzi, N. (2010). “Transverse Resistance of Masonry Infills.” ACI Structural Journal, 7.

Morandi, P., Hak, S., and Magenes, G. (2013). “Simplified out-of-plane resistance verification for slender clay masonry infills in RC frames.” Proceedings of the XV ANIDIS, L’Ingegneria Sismica in Italia, Padua.

Moreno-Herrera, J., Varela-Rivera, J., and Fernandez-Baqueiro, L. (2016). “Out-of-Plane Design Procedure for Confined Masonry Walls.” Journal of Structural Engineering, 142(2), 04015126.

Papia, M., L. Cavaleri, and M. Fossetti. (2003). “Infilled frames: Developments in the evaluation of the stiffening effect of infills.” Structural Engineering and Mechanics, 16 (6), 675–693. https://doi.org/10.12989/sem.2003.16.6.67.

Paulay, T., and Priestley, M. J. N. (1992). *Seismic Design of Reinforced Concrete and Masonry Buildings*. John Wiley and Sons, Inc., New York.

Pereira, M. F. P., Pereira, M. F. N., Ferreira, J. E. D., and Lourenço, P. B. (2011). "Behavior of masonry infill panels in RC frames subjected to in plane and out of plane loads." 7th international conference on analytical models and new concepts in concrete and masonry structures, 20.

Polyakov, S.V. (1960). "On the Interaction between Masonry Filler Walls and Enclosing Frame When Loading in the Plane of the Wall." Translation in Earthquake Engineering. Earthquake Engineering Research Institute 36–42.

Pradhan, B., and Cavaleri, L. (2020). "IP-OOP interaction in URM infilled frame structures: A new macro-modelling proposal." Engineering Structures, 224, 111211.

Ricci, P., De Luca, F., and Verderame, G. M. (2011). "6th April 2009 L'Aquila earthquake, Italy: reinforced concrete building performance." Bulletin of Earthquake Engineering, 9(1), 285–305.

Ricci, P., Di Domenico, M., and Verderame, G. M. (2018a). "Experimental assessment of the in-plane/out-of-plane interaction in unreinforced masonry infill walls." Engineering Structures, 173, 960–978.

Ricci, P., Di Domenico, M., and Verderame, G. M. (2018b). "Experimental investigation of the influence of slenderness ratio and of the in-plane/out-of-plane interaction on the out-of-plane strength of URM infill walls." Construction and Building Materials, 191, 507–522.

Ricci, P., Di Domenico, M., and Verderame, G. M. (2019). "Nonlinear dynamic assessment of the out-of-plane response and behaviour factor of unreinforced masonry infills in reinforced concrete buildings." Proceedings of the 7th International Conference on Computational Methods in Structural Dynamics and Earthquake Engineering (COMPDYN 2019), Institute of Structural Analysis and Antiseismic Research School of Civil Engineering National Technical University of Athens (NTUA) Greece, Crete, Greece, 2103–2115.

Saneinejad, A., and Hobbs, B. (1995). “Inelastic Design of Infilled Frames.” Journal of Structural Engineering, Vol. 121(Issue 4).Sim, C., Rautenberg, J., Schultz, A., Mustafraj, E., Penava, D., and Abrahamczyk, L. (2020)."Building Survey in Durrës after the 2019 Albania Earthquake," Virtual Presentation at the ACI Committee 133 - Disaster Reconnaissance, Rosemont, IL, Mar. 29-Apr. 2.

Stafford Smith B., and Carter, C. (1969). “A method of Analysis for Infilled Frames.” Proceedings of the Institution of Civil Engineers, 31–48.

Spesdar, R. (2017). “Experimental investigation on the out-of-plane behaviour of the concrete masonry infilled RC frames.” MSc, Dalhousie University, Halifax, Nova Scotia.

Varum, H., Furtado, A., Rodrigues, H., Dias-Oliveira, J., Vila-Pouca, N., and Arêde, A. (2017). “Seismic performance of the infill masonry walls and ambient vibration tests after the Ghorka 2015, Nepal earthquake.” Bulletin of Earthquake Engineering, 15(3), 1185–1212.

Verlato, N., Guidi, G., and Da Porto, F. (2014). “Experimental testing and numerical modelling of infill masonry walls subjected to in-plane damage.” 9th International Masonry Conference, Guimaraes, Portugal.

Wang, C. (2017). “Experimental investigation on the out-of-plane behaviour of concrete masonry infilled frames.” MSc, Dalhousie University, Halifax, Nova Scotia.

Wang, X., Zhao, W., Kong, J., and Zhao, T. (2020). “Numerical Investigation on the Influence of In-Plane Damage on the Out-of-Plane Behavior of Masonry Infill Walls.” Advances in Civil Engineering, 2020, 1–16.

Zahrai, S. M., Moradi, A., and Moradi, M. (2015). “Using friction dampers in retrofitting a steel structure with masonry infill panels.” Steel and Composite Structures, 19(2), 309–325.